Counterpoint deposition in the Netherlands: a case study of the Waal River by Nijmegen

MSc Thesis, Wageningen University and Research, SGL80436

Study Programme: Master of Earth and Environment: Soil Geography and Land Surface Dynamics

Author: Lisa Boterman

Supervised by: Jasper Candel & Bart Makaske

9 May 2022

Abstract

Channel deposits from meandering rivers have proven to be far more complex than the well-known lithofacies model consisting of sandy channel, gravelly channel-lag, and silty overbank deposits. This is especially relevant for sharp bends in rivers, which are subject to different meander behaviour than bends with lower curvatures; sharp bends are instead often accompanied by zones of flow separation which enable deposition of sediment in the outer bend. This phenomenon is known as counterpoint deposition, forming counterpoint bars. In this research, the scroll bar morphology associated with a sharp bend in the Waal river near Nijmegen is investigated for the potential that counterpoint deposits are present, as opposed to the current paleogeographic reconstruction that considers these deposits to be part of a point bar complex. This hypothesis is tested through means of borehole descriptions, optically stimulated luminescence (OSL) dating, and ground penetrating radar (GPR). It is concluded that counterpoint deposits are present at this location; the identified deposits consist of clays and sandy clays with fine sand laminations, and sporadic larger sand bodies. These grade upstream into point bar deposits dominated by coarser sands with gravels, and occasional clay and plant material layers. These lithologies and their stratigraphic relationships match those described in previously studied counterpoint deposits and their point bar counterparts. OSL dates reveal a direction of deposition towards the present channel location, indicating previous downstream migration of the paleochannel bend that is commonly associated with counterpoint deposition. This chronology excludes the possibility that the scroll morphology is part of a point bar, since this scenario would require the chronology to be reversed. These results offer a new paleogeographic interpretation for evolution of this meander bend in the Waal, and have implications for the recognition of counterpoint deposition in Dutch fluvial systems. Further research to improve our understanding of counterpoint deposition is required to contribute the successful management and restoration of our rivers systems.

Contents

1. Introduction

Understanding river dynamics, channel morphology and fluvial processes is essential in a country such as the Netherlands, where proximity to water bodies has made river and stream management an inherent part of society. The hydraulic and geomorphic conditions responsible for channel patterns are especially relevant to understand for the sustainable management of rivers and streams (Brierley & Fryirs, 2009; Candel et al., 2021). The alluvial plain of the Rhine Meuse delta system comprises a large part of the Netherlands and presently consists of meandering rivers which are laterally fixed by dikes and groynes. The topographic and subsurface characteristics of channel belts in this alluvial plain largely define the landscape identity and have an extensive effect on spatial planning. Meandering channel deposits, however, have proven to be far more complex than the well-known lithofacies model consisting of sandy channel, gravelly channel-lag, and silty overbank deposits (Makaske & Weerts, 2005; Sylvester et al., 2021).

It is becoming widely recognized that fine deposits within a floodplain do not solely consist of overbank deposits, but that they can also form a substantial part of channel deposits (Makaske & Weerts, 2005). Nanson (1980) found that in sharper river bends, sediments on the downstream side of coarser-grained point bars become progressively finer. Page & Nanson (1982) demonstrated how flow expansion at sharply curved meanders, and subsequent concave (outer) bank accretion also contributes to floodplain formation. More recently, concave bank deposition has been demonstrated to be an autogenic process in meandering rivers, occurring wherever short, high curvature bends are present (Sylvester et al., 2021). In-channel sedimentation in the outer bend of a river is known as counterpoint deposition or counterpoint accretion, forming so-called counterpoint bars (Makaske & Weerts, 2005; Smith et al., 2009, 2011, Kleinmans et al., in press). Studies have shown that counterpoint bar formation often takes place under conditions where a river encounters erosion-resistant material in a sharp outer bend (Makaske & Weerts, 2005; Smith et al., 2009).

These conditions for potential counterpoint bar formation are met at a sharp bend in the Waal river flanking the Ooijpolder near Nijmegen, where a Saalian aged (238-128 ka) ice-pushed ridge provides erosion-resistant material on the outer bank (Fig. 1). Several paleogeographic reconstructions for the evolution of this meander bend during Roman times exist, all of which include some manner of meander bend migration by point bar formation in a SE direction at the foot of the ice-pushed ridge, followed by cut-off of this bend around Roman times (Berendsen & Stouthamer, 2000; Cohen et al., 2012; Willemse, 2019; Heunks & van de Geer, 2021). However, this interpretation is unable to satisfactorily clarify the locations of multiple Roman-aged archeological findings in Nijmegen. Several phases of Roman fortifications located on the ice-pushed ridge dating between 19 BC and 105 AD were found to have moved westward over this relatively short period of time (Willemse, 2019). Based on other Roman fortifications in the Netherlands (e.g. Alphen aan den Rijn, Bodegraven) it is known that it was preferred to build these as close as possible to the river, despite there often being more topographically strategical locations available (Daniel, 2016). Given also the sharpness of this river bend, and its proximity to a steep ice-pushed ridge formed of material that is topographically and thus physically difficult to erode, it is possible that different flow dynamics from those in a typical smooth meander occurred, resulting in counterpoint deposition and downstream instead of lateral

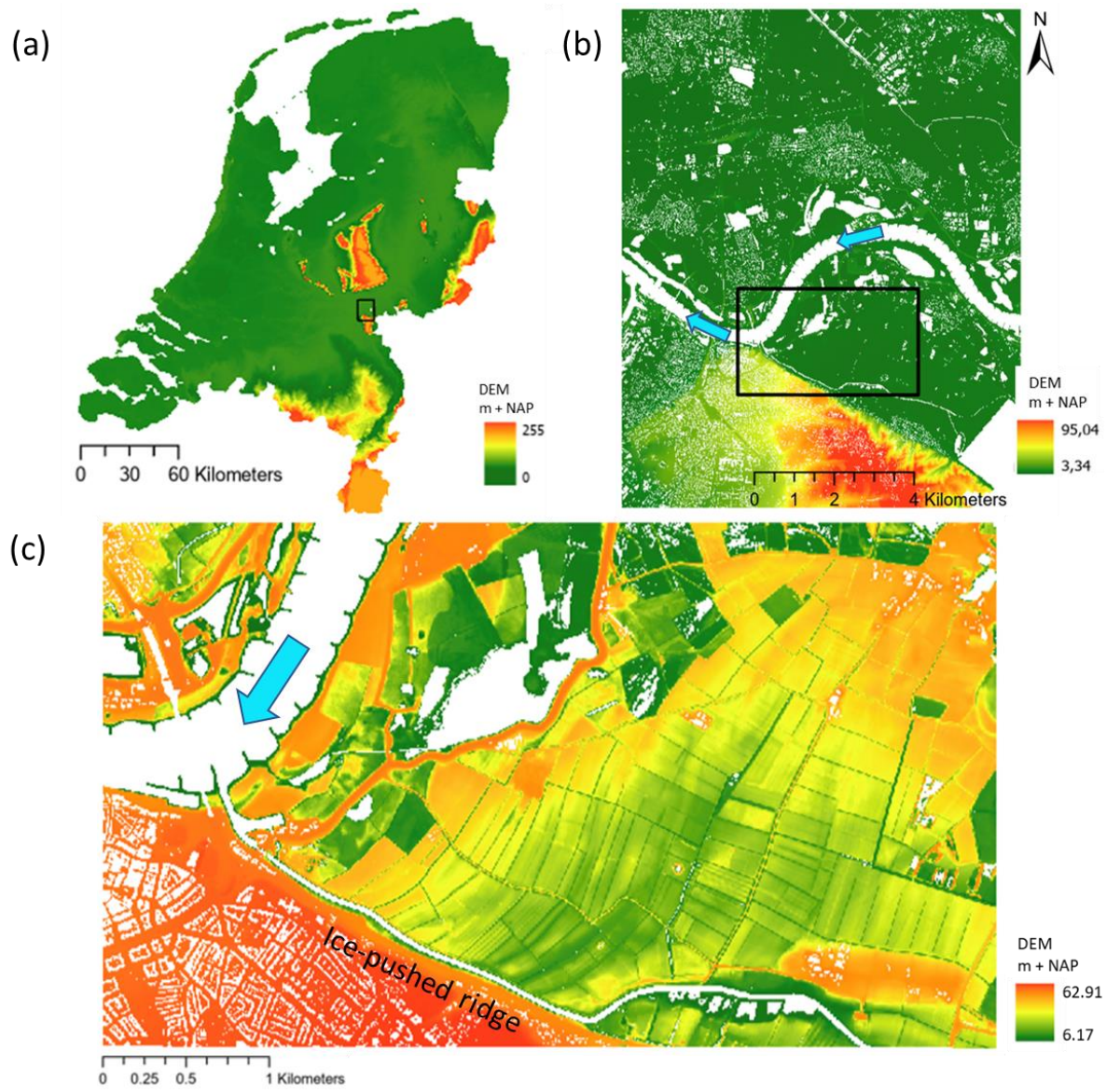

Figure 1: Digital elevation model showing (a) the study region location in the Netherlands (AHN2); (b) the study area NE of the ice-pushed ridge at the bottom of the picture (orange) and SE of the sharp bend in the Waal river (AHN3); and (c) the (SW) Ooijpolder with visible scroll bar morphology to the NE of the ice-pushed ridge (AHN3). Blue arrows indicate the direction of flow of the Waal river.

migration of the meander bend. This raises the question whether previously accepted palaeogeographical interpretations of the associated deposits are correct, or whether these deposits are instead counterpoint deposits, which might better fit the archaeological and geomorphological context. Indeed, Makaske & Weerts (2005) conclude that counterpoint bar deposits can easily be mistaken for deposits from natural levees or residual channels.

Recognition of counterpoint deposition in the Netherlands is limited to just two studies (as far as we are aware). Makaske & Weerts (2005) identified 5-6m thick successions of counterpoint deposits along the margins of the Hennisdijk channel belt, an abandoned Rhine distributary dating between 3800-3000 BP. Candel et al. (2020) identified counterpoint deposits in the Dommel system along valley margins and upstream of concave banks dating between 8.5-2.5 ka. Given the extent of waterways within the Netherlands, there is distinct potential for counterpoint deposits going

unrecognized in our fluvial landscapes. This could have several implications for the increasingly occurring river restoration projects across the country, as well as for spatial planning. Rather than lateral expansion of a river bend as considered typical for a meandering planform, downstream migration takes place in sharp bends where outer banks are erosion-resistant, which could have implications for the planning of restoration projects, and for spatial planning in general. Sharp bends and the resulting recirculation and stagnation of flow near the outer bank enable sediment deposition and plant growth (Schnauder & Sukhodolov, 2012), thereby creating habitat, shelter and spawning zones for aquatic species. The recognition of such areas associated with flow expansion and recirculating zones in outer bends are often ignored in spatial planning and in stream restoration practices (Kleinmans et al., in press). It is therefore very relevant that the various processes associated with counterpoint deposition are accounted for in our co-existence with, and management of, rivers.

In this research, we hypothesized that instead of a meander cut-off of the Roman aged river bend in the Ooijpolder having occurred, downstream migration of this meander bend to the NE along the ice-pushed ridge took place, resulting in counterpoint deposition. This was tested through (1) determining the extent of fine sediments present in the study area and their resemblance to previously identified counterpoint deposits; (2) gathering chronological evidence for the time of deposition of sediments relative to their position within the study area, which is currently lacking (Willemse, 2019); and (3) by assessing the internal structure of the scroll bar deposits to identify the direction in which sediment accretion took place. The following research questions are answered:

1. What types of sediments are found in the scroll bar morphology in the SW of the Ooijpolder, and are these typical of point bar deposits as postulated in current paleogeographic reconstructions?
2. Using the chronostratigraphy of these deposits, what was the direction of movement of the sub-recent Waal (since Roman times) at the foot of the ice-pushed ridge?
3. Can the internal structure of the scroll bar complex be used to indicate the sediment accretion direction and associated channel migration that took place in the SW of the Ooijpolder?

2. Background

2.1. Counterpoint bar formation

Counterpoint bars describe the fine-grained, muddy or clayey counterparts to point bars that form at the downstream tail of a point bar and in the concave (outer) bank of the river (Fig 2; Page & Nanson, 1982; Nanson & Croke, 1992). Previously, the terms concave bank bench (Page & Nanson, 1982; Nanson & Page, 1983), counterpoint accretion (Nanson & Croke, 1992; Makaske & Weerts, 2005) and counterpoint bars (Smith et al., 2009, 2011) have been used. This study will use the term counterpoint bar to refer to such deposits. Counterpoint bar formation occurs in conditions involving tightly curved meander bends (Page & Nanson, 1982; Nanson & Croke, 1992; Smith et al., 2009), which often form where material on the outer bank of the river is erosion-resistant. This can take place in confined meander belts developing in a valley that limits floodplain width, or where the

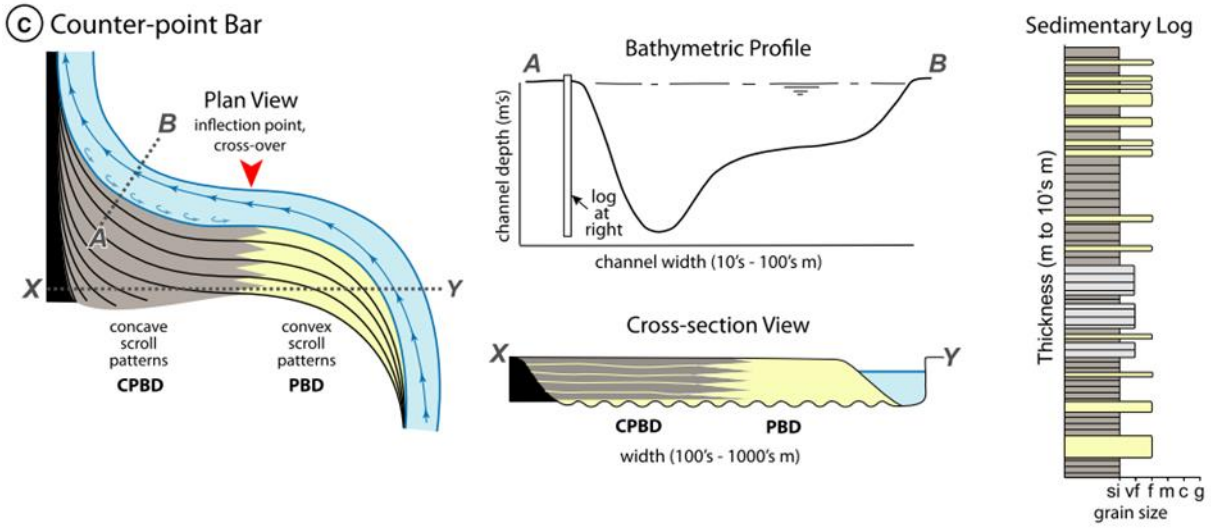

Figure 2: Plan view and cross-sectional view, bathymetric profile and sedimentary log of typical counterpoint bar deposits; note the S shaped surface expression of scrolls around the inflection point and transition from fine to coarser sediment. CPDB= counterpoint bar deposits; PBD= point bar deposits. From Durkin et al. (2020).

laterally migrating channel encounters mud-filled channels or oxbows that prove too cohesive to erode (Smith et al., 2009). Low stream power can also facilitate counterpoint deposition when there is insufficient erosive capacity for lateral expansion of a meander bend, resulting in counterpoint deposition and subsequent downstream migration of the meander (Nanson & Page, 1983; Makaske & Weerts, 2005).

These sharp bends in rivers are often accompanied by zones of flow separation due to complex shear stresses and pressure gradients as bend curvature increases (Nanson, 1980; Blanckaert, 2011; Kleinmans et al., in progress). This flow separation causes recirculation of water in the outside bend of the river (Fig. 2) and reduced flow velocity, enabling deposition of sediment, whereas in a typical meander, sediment in the outside bend is eroded (Makaske & Weerts, 2005; Smith et al., 2009, 2011). Reduced flow velocity present in these zones enables deposition of fine and suspended sediment, and as such, counterpoint bars are often noticeably different from point bars in their lithology, consisting largely of silts and clays, often with a relatively high organic matter content (Nanson & Croke, 1992; Smith et al., 2009). A gradational boundary between a point and counterpoint bar forms around the inflection point due to the slow transition in convex curvature of a point bar to concave curvature of a counterpoint bar (Sylvester et al., 2021). Accretion of a counterpoint bar takes place as a series of concave ridges along the concave bank of the river (Sylvester et al., 2021). These are distinguishable from point bar deposits in their surface morphology that arc in the upstream direction, compared to point bar scroll patterns which often arc in a downriver direction (Fig. 3; Smith et al., 2009). This accretion results in downstream migration of the meander bend as opposed to lateral migration associated with point bar formation.

2.2. Study Area

The Waal river is a sand-bed distributary of the river Rhine, which splits into the Waal and the Pannerden canal about 5 km downstream of Lobith. The average discharge of the Rhine at Lobith is 2300 m^3/s (Middelkoop & Haselen, 1999), with the Waal receiving two-thirds of this discharge. The

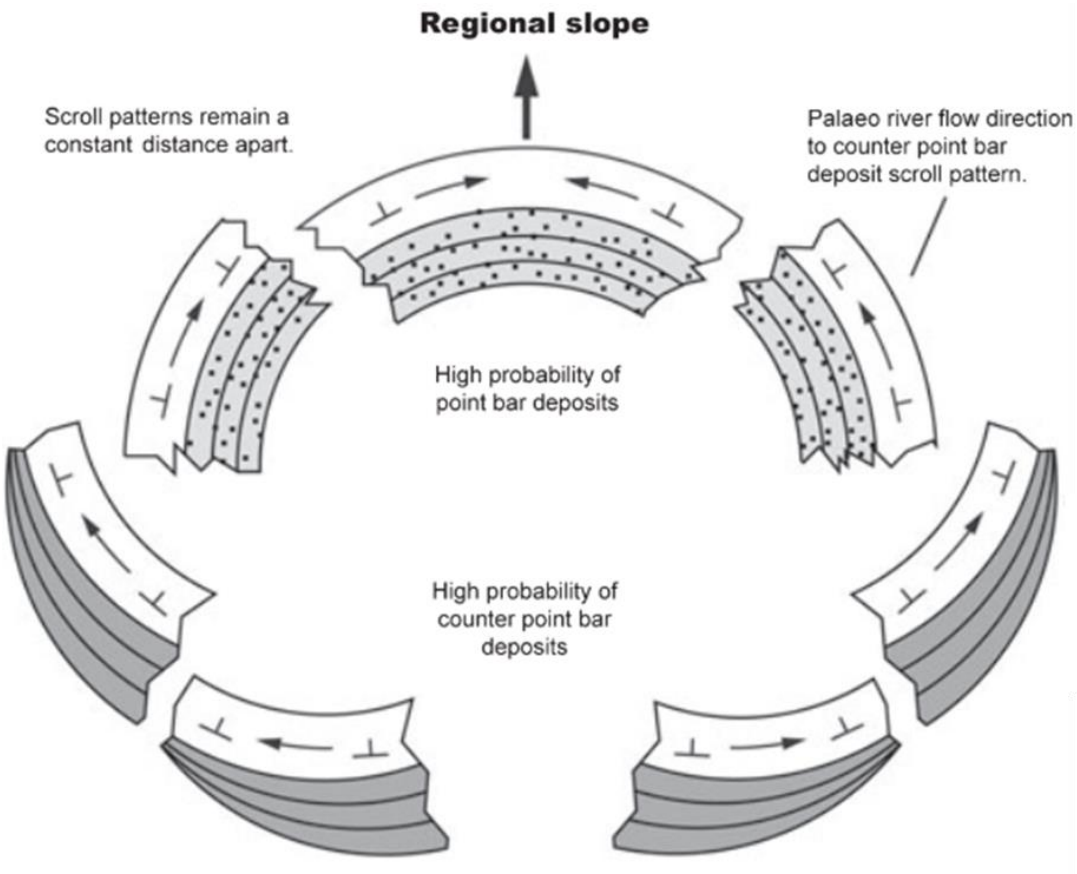

Figure 3: Schematic diagram showing scroll patterns of point bar deposits (top) and counterpoint bar deposits (bottom) relative to flow direction and regional slope (arrows). Note how counterpoint deposits merge together. From Smith et al. (2009).

Waal river currently has a depth of around 3 m and is 300-400 m wide during average flow conditions (Hobo et al., 2014). Presently, the river is bounded by dikes, the completion of which took place in the study area around 1325 AD (Willemse, 2019). Prior to this, the Waal was a freely meandering river (Middelkoop & Haselen, 1999; Hobo et al., 2014; Willemse, 2019). At Nijmegen, south of the Waal river, remnants of an ice-pushed ridge remain (Fig. 1c), which formed during the Saalian glacial from pre-Saalian fluvial sediments (Daniel, 2016).

The study area is located in the Ooijpolder to the SE of the Waal river and NE of the ice-pushed ridge (Fig. 1). This area encompasses a (presumed) point bar complex with visible scroll bar morphology (Fig. 4), formed by a Roman-aged meander bend of the Waal river. Scroll bars are defined by Mason & Mohrig (2019) as constructional, rather than erosive, features that are deposited on top of point bars, with swales resulting from negligible deposition compared to that forming scroll bar crests. Once established, swales may channel overbank flows which then erode sediment between scroll bars. This definition does not necessarily describe the surface morphology seen in the study area, however, the term scroll bars will be used throughout to avoid ambiguity. The study area is bound by late-Pleistocene aged sediments to the east of Persingen (Cohen & Stouthamer, 2012; Willemse, 2019), while Roman-aged archaeological finds provide a delineation of the study area north of Persingen, given these finds were preserved in-situ (see Fig. 4 for locations; Thijssen & Wildenberg, 2005). This delineation is further supported by a pre-Roman aged remnant channel found to the north of Persingen (Fig. 4); a comparable remnant channel north of the current Waal has been found

that dates to 400-100 BC. Based on these infilled channels, the bankfull width of the river during Roman times is estimated to be between 150-200m, with a depth of around 6m (Willemse, 2019).

2.3. Previous paleogeographic reconstructions

Multiple paleogeographic interpretations of the development of the study area exist. Willemse (2019) stated that the system within the Ooijpolder became active from 600 BC onwards, with particular emphasis on a supposed remnant channel 'visible' in the scroll bar morphology that, based on a ^{14}C dating was filled in by 131-260 AD (see Fig. 4 for location). Cohen & Stouthamer (2012) dated this meander system within the Ooijpolder, and the (presumed) associated paleochannel to have had its channel infilling between 2500-1800 BP, based on a combination of a ^{14}C dating and archaeological and historical evidence (Willems, 1986; Cohen et al., 2012). Berendsen & Stouthamer (2000) referred to the "present" river Waal having come into existence shortly after 2000 BP, also suggesting abandonment of its presumed previous course around this time. Willems (1986) suggested that the Roman Waal flowed in approximately the same location as in the present, following a short period (a few centuries) of activity within the Ooijpolder before Roman times.

Heunks & van de Geer (2021) proposed a different paleogeographic interpretation of the study area based on several borehole transects and ^{14}C dates, involving two phases of lateral meander bend expansion into the Ooijpolder and subsequent bend cut-off (Fig. 4). The first of these phases identifies the same paleochannel as in Willemse (2019) based on a borehole transect in the east of the study area along the Persingsestraat, with the interpretation of chute cut-off taking place around

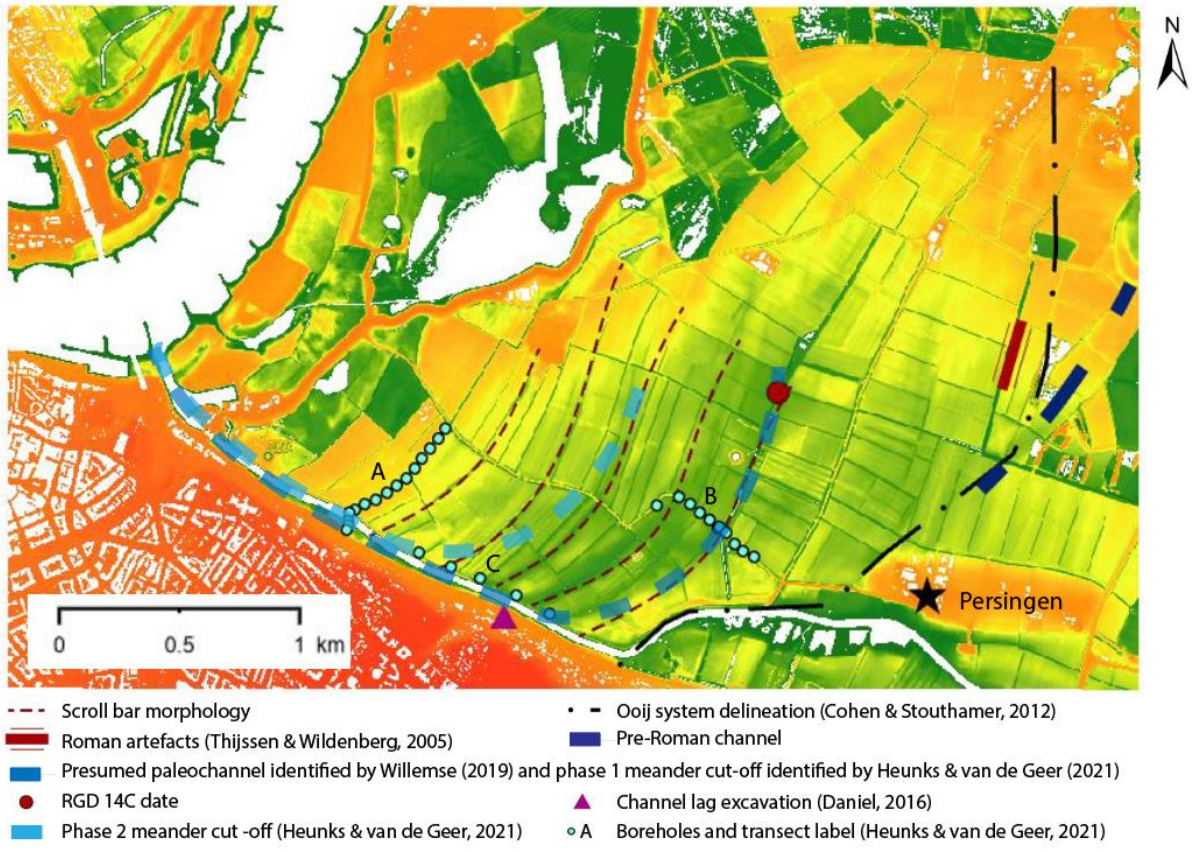

Figure 4: Digital elevation model (AHN3) showing the study area with visible scroll morphology in the surface and locations of interest from previous research.

40 BC and subsequent infilling of the channel. The second phase of this reconstruction is based on a series of younger ^{14}C dates found further NW (for further discussion see Section 5.4) and closer to the present river, where it is postulated that after cut-off of the older channel, a new phase of lateral expansion towards the SE began that was then also cut off around 500 AD (Fig. 4).

A canalized waterway 'het Meertje' runs beneath the ice-pushed ridge in the location where the (pre) Roman-aged channel of the Waal is presumed to have run (Fig. 4). The age of this waterway, however, is still unclear (van den Broek et al., 2009). Mulder (2008) refers to this waterway probably having existed since Roman times, and being canalized in the 17th century, while Driessen (2007) contemplates presence of het Meertje to have influenced construction of the Roman military camp located on the Hunerberg, atop the ice-pushed ridge (Fig. 5). In contrast, Willemse (2019) suggests that beneath the ice-pushed ridge a swampy area existed that was fed by seepage water from the ice-pushed ridge and by water sourced from the SE during high river flows, and that later a waterway was dug here. Other sources indicate that the Waal river did indeed flow beneath the ice-pushed ridge due to meander expansion into the Ooijpolder during the early-mid Iron age (from c. 800 BC). Heunks & van Hemmen (2016) suggested that presence of the channel beneath the ice-pushed ridge resulted in erosion of gravel-rich material, which can be seen in point bar deposits further downstream. They consider, however, that in Roman times, the channel was in the process of infilling, having been cut off prior and forming a secondary waterway connected to the Waal downstream that was perhaps kept open by the Romans to use as a harbour. A study by Daniël (2016) that sought to discover the location of the Roman harbour by means of excavation at the foot of the ice-pushed ridge (for location see Fig. 4), however, did not find any evidence of a harbour, having reached channel lag at a depth of 5.8m (Willemse, 2019).

2.4. Archeological context

An overview of Roman settlements and military camps occupied from 19 BC to the 5th century AD is shown in Fig. 5. Notable about these settlements is that their occupation was never continuous, but rather a series of military camps and civilian settlements were built over and occupied for a relatively short period of time. The first Roman occupation of Nijmegen took place with the building of a military camp atop the Hunerberg in 19 BC, that was in use until 12 BC (van der Heijden, 2016). Towards the end of this period, additional military camps were built around 400 m to the east on the Kops Plateau where it is thought administrative tasks were centred (Driessen, 2007; van der Heijden, 2016). At the same time, a civilian settlement *Oppidum Batavorum* was built at the location of the present Valkhof. Construction at Kops Plateau was renewed between 13-16 AD, while several temporary military camps were built around the present Traianusplein, Oranjesingel and Koningsplein (van der Heijden, 2016). The military camp at the Hunerberg was re-occupied by a Roman legion around 70 AD after the Batavian revolt and destruction of *Oppidum Batavorum*, until 104 AD when this legion was sent to fight in the Dacian wars (Willems, 1990). At the same time as re-occupation at the Hunerberg, a new civilian settlement *Ulpia Noviomagus* was built in the present Waterkwartier in Nijmegen-West. Driessen (2007) suggested this settlement became a centre of trade almost certainly associated with a harbour near this location. *Ulpia Noviomagus* and several other settlements remain occupied until around 270 AD, after which the fall of the Roman *limes* saw

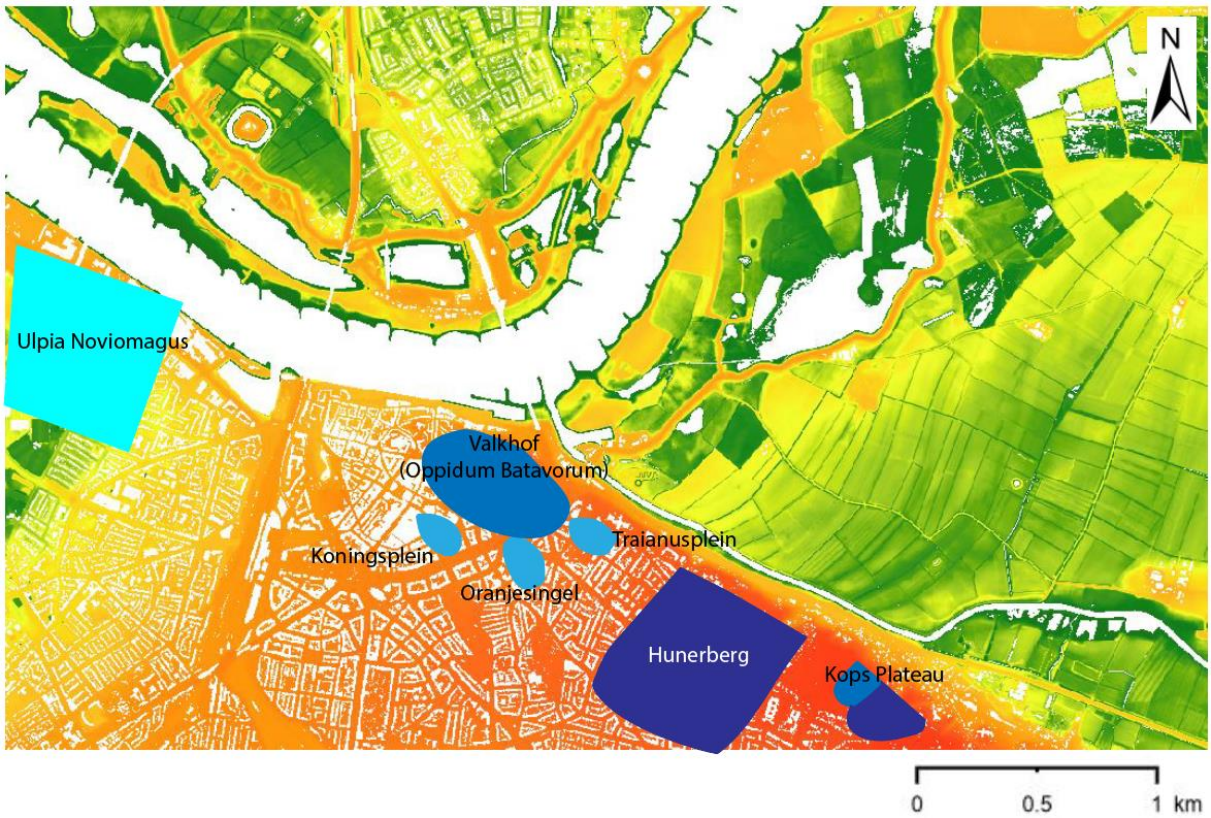

Figure 5: Overview of the main Roman military camps and settlements discovered in Nijmegen. Darker blue colours correspond to the older settlements and lighter blue to the younger ones. Adapted from Willemse (2019).

a reduction in settlement, with the only remaining occupation centred at the present Valkhof (Willems, 1990). By 450 AD the fall of the Roman empire saw the end of Roman occupation in Nijmegen and in the Netherlands.

That a Roman harbour existed in Nijmegen is an almost certain fact given the variety of archaeological findings that indicate trade of commodities such as grain, olive oil, wine and pottery (Daniël, 2016). Additionally, the discovery of several brick ovens dating to the 1st and 2nd century AD in Berg and Dal (further SE along the ice-pushed ridge), and their recovery across the Netherlands suggest transport by means of shipping (Willems, 1990). The lack of continuous occupation of the abovementioned Roman settlements has led to suggestions that external factors such as migration of the river was responsible for the Roman's frequent relocation within Nijmegen (Daniël, 2016; Willemse, 2019). Assuming a harbour was present from around 70 AD at *Ulpia Noviomagus* as Driessen (2007) suggested, it follows that an older Roman harbour may lie elsewhere that served during their period of occupation prior to 70 AD. Given their preference for building close the river over more topographically strategic locations as demonstrated by other Roman fortifications in the Netherlands (Daniël, 2016), and based on the locations of their oldest military settlements, this potential harbour could be located somewhere at the foot of the ice-pushed ridge. The analysis of van der Heijden (2016) supports this theory; it was estimated that the earliest camp at the Hunerberg was occupied by three Roman legions, totalling around 15,000 men. To be able to feed such a number would logistically have been extremely challenging without a well organised shipping network having been also established immediately upon their occupation at Nijmegen.

3. Methodology

3.1 Existing data

An existing dataset of lithological borehole descriptions compiled by H.J.A. Berendsen and physical geography students of Utrecht university between 1972-2012 (Cohen, 2017) is available and was used to gain an overview of the study area prior to fieldwork to discern any already apparent lithological trends. However, given the potential for inconsistencies in this dataset due to compilation many different people, and the fact that in most cases boreholes are of insufficient depth for our purposes, these descriptions were not utilized further.

Until recently, there was a relative scarcity of dated locations within the Ooijpolder, with just one ^{14}C dating existing from 1983 by the Netherlands Geological Survey (RGD; De Jong, as cited by Willems, 1986). Heunks & van de Geer (2021) made a significant contribution to this with their study providing an additional 11 ^{14}C ages from six locations at various depths. These data are compared with our own results from OSL dating to give a more comprehensive chronological overview of the area.

3.2 Lithological borehole descriptions

Two transects (A and B) were delineated across the study area (Fig. 6a). Transect A is 1785 m long, has a NW-SE orientation and is positioned perpendicular to the scroll bar morphology visible in the digital elevation model (DEM), and also to the potential paleochannel shown in the evolutionary models by Willemse (2019) and Heunks & van de Geer (2021; Fig. 4). Transect B is 2175 m long, and has a SW-NE orientation across the hypothesized counterpoint to point bar transition, starting at the foot of the ice-pushed ridge. A total of 19 boreholes were made (Appendix 1), with each transect consisting of ten boreholes (one borehole overlaps both transects). Borehole locations were dependent on where permission by the landowners was given to access their land, and therefore the distance between boreholes varies. Depths of boreholes ranged between 3.2-6.3m. Across the potential paleochannel in Transect A and in the middle of Transect B where the hypothesized inflection point lies, boreholes were made closer together than across the rest of the transect.

The surface elevation and location of each borehole site was measured using RTK (real time kinematic positioning)-GPS. Boreholes were made using an Edelman auger (unsaturated sand), a gouge auger (clay) or a Van der Staay suction corer (saturated sand), depending on the type of sediment encountered. Descriptions of each borehole were made for 10cm intervals using the procedure of Berendsen & Stouthamer (2000) and the Dutch classification system (De Bakker & Schelling, 1966), including texture, median sand grain size (if applicable), OM (organic matter) content, plant material, colour, gravel (>2mm) content, Ca content and oxidation/reduction mottling. Sand grain size was measured in the field by visual comparison with a sand ruler. Additional observations such as layering or distinct differences within the 10cm interval were also recorded.

Borehole data was plotted in the programme LLG 2012 (Cohen, 2012) and used to draw lithological cross-sections of the sub-surface across transects A and B. Based on lithological characteristics, several facies were then identified and described. Interpretation of their lithogenesis took into account the depositional environments associated with these lithologies, stratigraphic relationships, the OSL results, and the surface morphology.

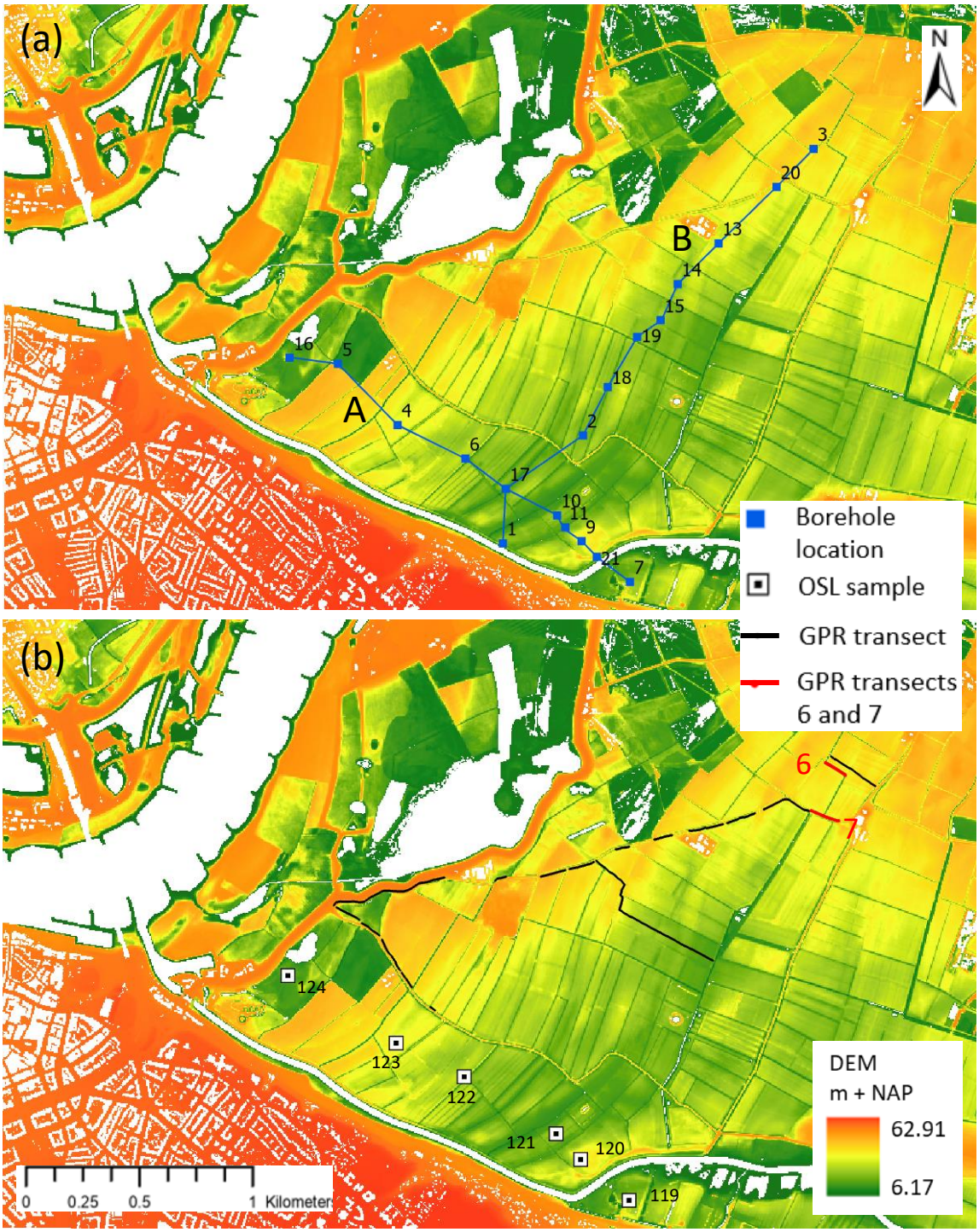

Figure 6: (a) Locations of transect A and B and the numbered borehole locations; (b) OSL sampling sites and abbreviated sample number (all are preceded by NCL2321), and GPR transects.

3.3. Optically Stimulated Luminescence dating

3.3.1. Theory

Optically Stimulated Luminescence (OSL) dating measures the luminescence signal that accumulates in buried quartz or feldspar grains due to naturally occurring radioactivity. This signal is a proxy for the time since the sediment was exposed to light (or buried), or the time since the sediment was exposed to temperatures exceeding 200˚C, both of which reset the luminescence signal (Preusser et al., 2008). This method is increasingly used to date fluvial sediments because the lack of in-situ

organic material can lead to age overestimation (in the case of transported material) or underestimation (where bioturbation has occurred) in the traditionally used radiocarbon dating (Wallinga, 2002).

Natural radiation received by sediments from surrounding sediments is sourced mainly from uranium, thorium and ^{40}K decay chains, as well as through cosmic radiation (Wallinga, 2002; Preusser et al., 2008). This radiation results in electrons being excited in a higher energy state, and can result in these electrons being trapped in defects within the crystal lattice. Subsequent exposure to light or heat releases these trapped charges, inducing a light flux in the form of photons (Wallinga, 2002). Measurement of this signal- the equivalent dose (De)- when the natural radiation, or environmental dose rate (DR), is known, enables calculation of the burial age of the sediment (Eq. 1):

$$age(ka) = paleodose\ (Gy)/dose\ rate\ (Gy\ ka^{-1}) \quad (1)$$

Following the single aliquot regenerative dose (SAR) protocol by Murray & Wintle (2000), the natural signal of the sediment grains is measured, and then compared to several known laboratory induced signals, or regenerative doses. Sensitivity of the signal may change after each regenerative dose, and therefore this is accounted for by administering a test dose to normalise the natural and each regenerative signal. The natural signal is interpolated from the sensitivity-corrected dose-response curve generated by administering known regenerative doses. More detailed explanations of the theory behind OSL and the SAR protocol can be found in Murray & Wintle (2000), Preusser et al (2008) and Rhodes (2011).

3.3.2. OSL Sampling

Six samples were collected for OSL dating (Fig. 6b). According to Preusser et al. (2008), OSL samples should be taken from a layer at least 50cm thick consisting of homogenous material to reduce the effect of non-homogenous radiation on dose-rate calculation. Sampling locations were therefore based on the borehole descriptions carried out prior to sampling to ensure there was sufficient sandy material present.

Samples were taken primarily in boreholes located in the higher-lying scroll bars of the scroll bar-swale morphology to avoid sampling potentially reworked sediment, and because the scroll bar sediments tended to contain thicker sand layers required for OSL. The exception to this was sample NCL2321-124 taken in borehole 16 where surface sediments have previously been excavated. Samples were taken below minimum groundwater levels to ensure moisture levels were most representative of average conditions since deposition. This prevents under or over-estimation of OSL signal given that pore water content dilutes the environmental dose rate received by sediments (Nelson & Rittenour, 2015). Sample depths ranged between 2.2-4.5 m below surface level (5.64-7.68 m +NAP). Distance between samples varied due to the abovementioned requirement for sufficiently thick sand layers to be present, and ranged between 160-560m. One of these samples (NCL2321-119) was taken to identify the boundary of the study area and was expected to form part of a river terrace deposit from the late Pleistocene/early Holocene (Cohen & Stouthamer, 2012; Willemse, 2019). Samples were taken using a Van der Staay suction corer following the method of Wallinga & Van der

Staay (1999), using 30cm PVC tubes, flexible lids and tape to seal the samples and prevent light exposure.

3.3.3. Sample preparation

Quartz samples were prepared for OSL measurement in the Netherlands Centre for Luminescence dating (NCL). The outer 3 cm of material in the sampling tubes that was likely exposed to light upon sampling was separated and prepared for environmental DR estimation (Section 3.3.4.). Material from within the tube that was not exposed to light was sieved to four fractions: >250µm, 212-250 µm, 180-212 µm, and <180 µm. The 212-250 µm fraction was used for further analysis, with the remaining fractions being stored in case not enough material of the chosen fraction was available. Samples were treated with HCl (10%; 1 hour 40 minutes) to remove carbonates, followed by H_2O_2 (10%; 48 hours) to remove OM. Given the presence of many micas and the dark colouring of the samples, samples were passed through an LB-1 Magnetic Barrier Laboratory Separator to obtain a more pure quartz sample; this was done at 1.4A, with each sample being passed through the separator twice. Samples were then treated with HF (40%; 45 minutes) to dissolve any feldspars and to etch the quartz grains, followed by another treatment with HCL (10%) to dissolve any salts formed in the previous step. Lastly, the samples were rinsed and dry-sieved through a 180µm sieve to separate out any partially dissolved feldspars while retaining the etched quartz grains.

3.3.4. Dose rate estimation

The material separated for DR estimation was dried overnight to enable measurement of water content, and then combusted at 500°C for eight hours to measure OM content. Measurements were made by weighing the material before and after each procedure, with the difference representing the water/OM content. Subsequently, samples were ground and sieved in order to obtain material of a homogenous grain size, then mixed with wax to form pucks of 2cm thickness. The pucks were analysed in the Rikilt laboratory using a high-resolution gamma ray spectrometer for activity concentrations of ^{40}K, U, and Th decay chains. Attenuation of radiation due to moisture and OM content were accounted for following the method of Aitken (1998). Given the potential for disturbance of sandy layers during sampling, water content of sandy samples was assumed to be 20% by weight with an error of 3%, corresponding to the average porosity of sand being 34% (Wallinga & Bos, 2009). Sample NCL2321-120 was noted to be clayey, and therefore the measured water content was used (32.5%) for this sample to calculate DR attenuation by water, albeit with a larger uncertainty of 7.5%. OM contents measured after combustion were used for the calculation of DR attenuation by OM. Cosmic ray contribution to dose rate was calculated based on Prescott & Hutton (1994), assuming instant burial for all samples.

3.3.5. Pre-tests

After sample preparation, several pre-tests were undertaken to ensure suitability of samples before measurement of the equivalent dose took place. Luminescence signal was measured on either a Risø TL/OSL DA15 reader delivering 0.1217Gy/s, or a Risø TL/OSL DA20 reader delivering 0.1447Gy/s at the sample position, both equipped with blue diodes and a Sr/Y source. The first pre-test was an IR test to determine whether the samples contained a luminescence signal and to assess if feldspar contamination was present. Given that both quartz and feldspars respond to stimulation by blue

light, this may cause an overestimation in the OSL signal if feldspars are present. However, feldspars also respond to stimulation under infrared (IR) light, while quartz does not (Preusser et al., 2008), and therefore incorporating this in the measurement sequence enables detection of feldspars. During this test, three aliquots per sample were stimulated with infrared light at 30°C after beta exposure to see whether the resulting signal differed from signal generated by beta exposure only; a lower OSL signal following IR exposure indicates whether feldspars are present (Wallinga et al., 2002). Feldspar contamination was not found in our samples.

A thermal transfer test was then conducted to determine pre-heat and cut-heat temperatures applied, before measuring the natural and regenerative signals respectively. Thermal transfer takes place when heating transfers electrons from light insensitive traps to the traps measured by OSL, which can then result in overestimation of the De (Cunningham & Wallinga, 2010; Wallinga et al., 2010). Given we expect (most) of the samples to be young and therefore have small De's, this phenomenon can be problematic due to its potentially relatively large effect on De. To test whether this effect was present in our samples, 24 aliquots each from samples NCL2321-120 and NCL2321-122 were tested at different pre-heat temperatures ranging from 180˚C to 280˚C (with 20˚C intervals, four aliquots per sample per pre-heat temperature) following bleaching by blue LED's at 30˚C for 300 seconds to reset the OSL signal. The temperature where excess signal was generated due to thermal transfer defined the pre-heat and cut heat temperatures, which for our samples were selected to be 200˚C and 180˚C respectively.

Lastly, a dose recovery test was conducted to test the assumption that OSL sensitivities of the test dose and preceding regenerative/natural dose are directly proportional (Wintle & Murray, 2006). This entailed resetting the OSL signal of the samples, then administering a known dose close to the expected age and measuring the resultant OSL signal. For sample 119 this dose was set at 100Gy, and for the remaining samples at 45Gy based on results from the initial IR test. The ratio of the administered dose to the measured OSL response was considered acceptable if it was between 0.9-1.1.

3.3.6. Equivalent (paleo) dose estimation

De was measured on small aliquots using the SAR protocol of Murray & Wintle (2000), detailed in Table 1. Where the natural signal exceeded the regenerative signals after following this protocol, additional regenerative doses (double the original beta test dose) were administered and measured to ensure the natural dose could be interpolated rather than extrapolated from the known regenerative signals.. A minimum of 21 aliquots per sample were measured, using a mask size of 2mm. Measurements were analysed using Risø Luminscence Analyst software using an early background subtraction protocol of Cunningham & Wallinga (2010). Aliquots with a maximum test dose error, recuperation signal, or feldspar contamination signal exceeding 10% of the measured signal were discarded, as well as samples with a recycling ratio outside the 0.9-1.1 range.

3.3.7. Age estimation

Given the requirement of luminescence dating for a grain's signal to be completely reset, using OSL to date fluvial sediments could arguably be unsuitable due to limited light exposure in some fluvial

settings (Wallinga, 2002). This is because in fluvial conditions with reduced light exposure under turbid water, grains may not be completely bleached at the time of deposition, which can lead to age overestimation (Quik & Wallinga, 2018). To account for potential heterogenous bleaching in our samples, a bootstrapped minimum age model (bsMAM; Galbraith et al., 1999) was applied to the preliminary De measurements, which truncates the distribution of De measurements to identify a minimum dose that is assumed to represent the dose of a well-bleached, or fully reset signal (Chamberlain et al., 2018). A required parameter for the MAM is the overdispersion or σ_b (representing variation in De estimates beyond the statistical model) of a well bleached sample. Since the degree of bleaching of our samples is not known, a calculated σ_b was used following the procedure of Chamberlain et al. (2018). This was obtained by running a bootstrapped central age model (CAM; Galbraith et al., 1999) on each sample to obtain the overdispersion per sample. Subsequently, a bsMAM was run on these resultant overdispersion values to obtain a single overdispersion value. This value was then used as input to run the bsMAM for each individual sample. The calculated σ_b used was 0.1127 with an error of 0.0492.

Table 1: SAR (single aliquot regenerative-dose) protocol followed to measure equivalent dose.

Step	Action	Measured dose
1	None/administer beta dose	
2	10s preheat at 200˚C	
3	OSL- 20s blue light stimulation 125 ˚C	Natural dose, test dose
4	Beta test dose	
5	10s cut-heat 180 ˚C	
6	OSL- 20s blue light stimulation 125 ˚C	Regenerative dose, test dose
7	40s blue light bleach 210 ˚C	
8	Repeat steps 1-7 for regenerative, recuperation and repeat regenerative doses	
9	Repeat steps 1-7 adding 20s IR bleach at 30 ˚C prior to step 3	

3.4. Ground Penetrating Radar

Ground penetrating radar (GPR) was used in attempt to identify lateral accretion surfaces to determine the direction of movement of the river. Measurements were conducted using a GSSI radar with a SIR4000 display systema and 200HS antennae. Several transects were surveyed in the northern part of the study area under the hypothesis that the presumed counterpoint deposition zone in the SW would be too clayey for successful GPR results. An initial transect perpendicular to the hypothesised CPB-PB transition across borehole 15 (Fig. 6) returned little signal, thus subsequent transects (Fig. 6b) were surveyed through the 1-2m deep ditches alongside parcels of land in attempt to maximise depth of the signal. The location of GPR transects was therefore largely dependent on accessibility of ditches, and often located roadside. Processing of the data took place using Reflexw software. Coordinate data were added to the profile, followed by setting the electromagnetic wave velocity (i.e. the reflected signal) at 0.08m ns^{-1} based on hyperbola fitting (Sandmeier, 2020). The functions DC shift, subtract-mean, static correction and gain were used to enhance the signal and thus the layer visibility. Further details on these methods can be found in Sandmeier (2020).

4. Results

4.1. Borehole cross-sections

Two lithological cross-sections were created based on the borehole descriptions of Transects A and B (Fig. 7). Several facies were identified within the lithological cross-sections A and B by analysing grain size trends and relative positioning of the deposits, as well as characteristics noted in the field (Fig. 8). Table 2 provides a summary of these facies.

Facies 1, in the SE of cross-section A, is subdivided into Facies 1a and 1b. Facies 1a is comprised of a clear fining up sequence that lacks in the rest of the study area. This sequence consists of non-calcareous medium to coarse-grained coloured sands (210-1000µm) that are in places poorly sorted

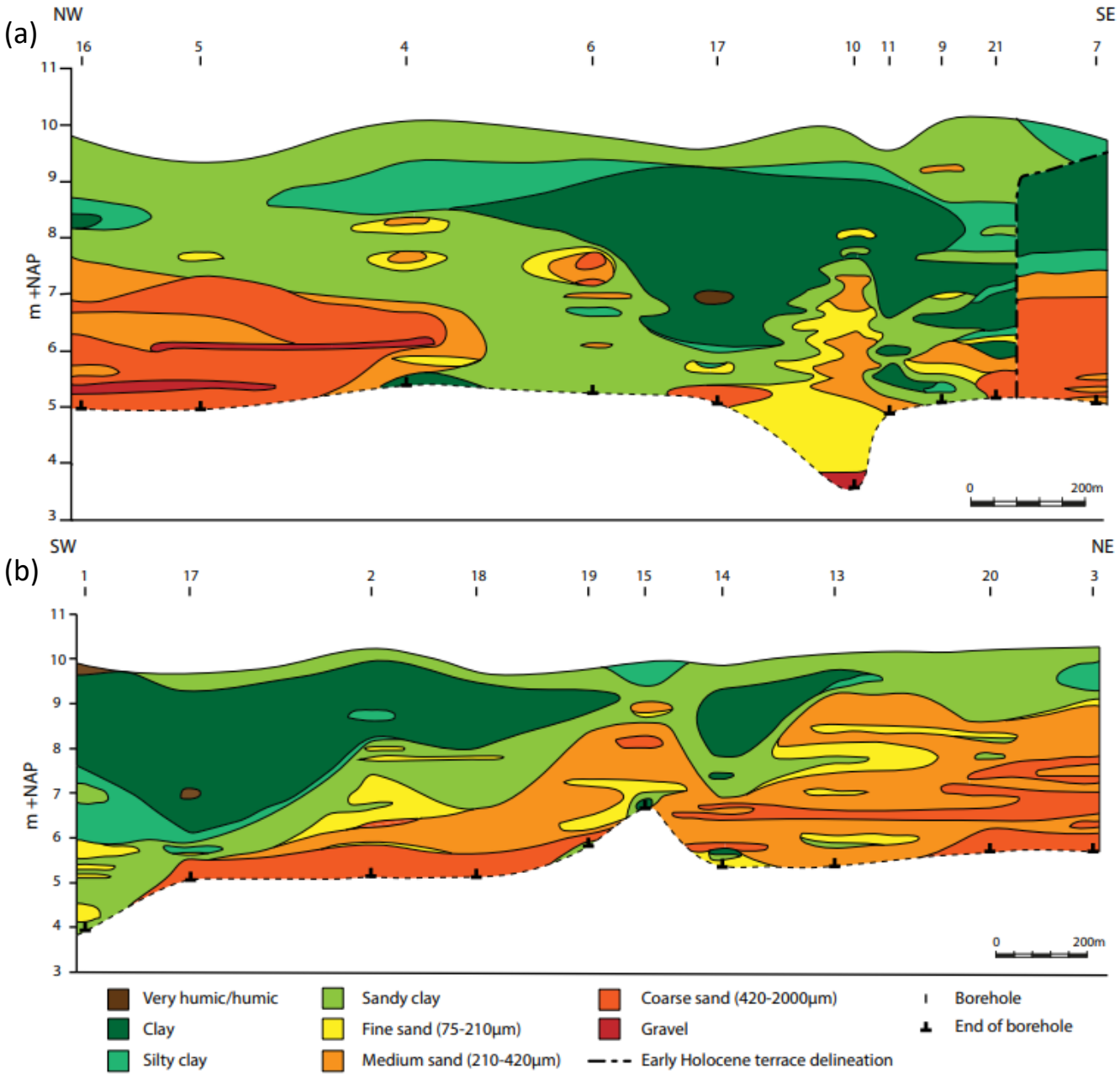

Figure 7: Lithological cross-sections for (a) Transect A and (b) Transect B.

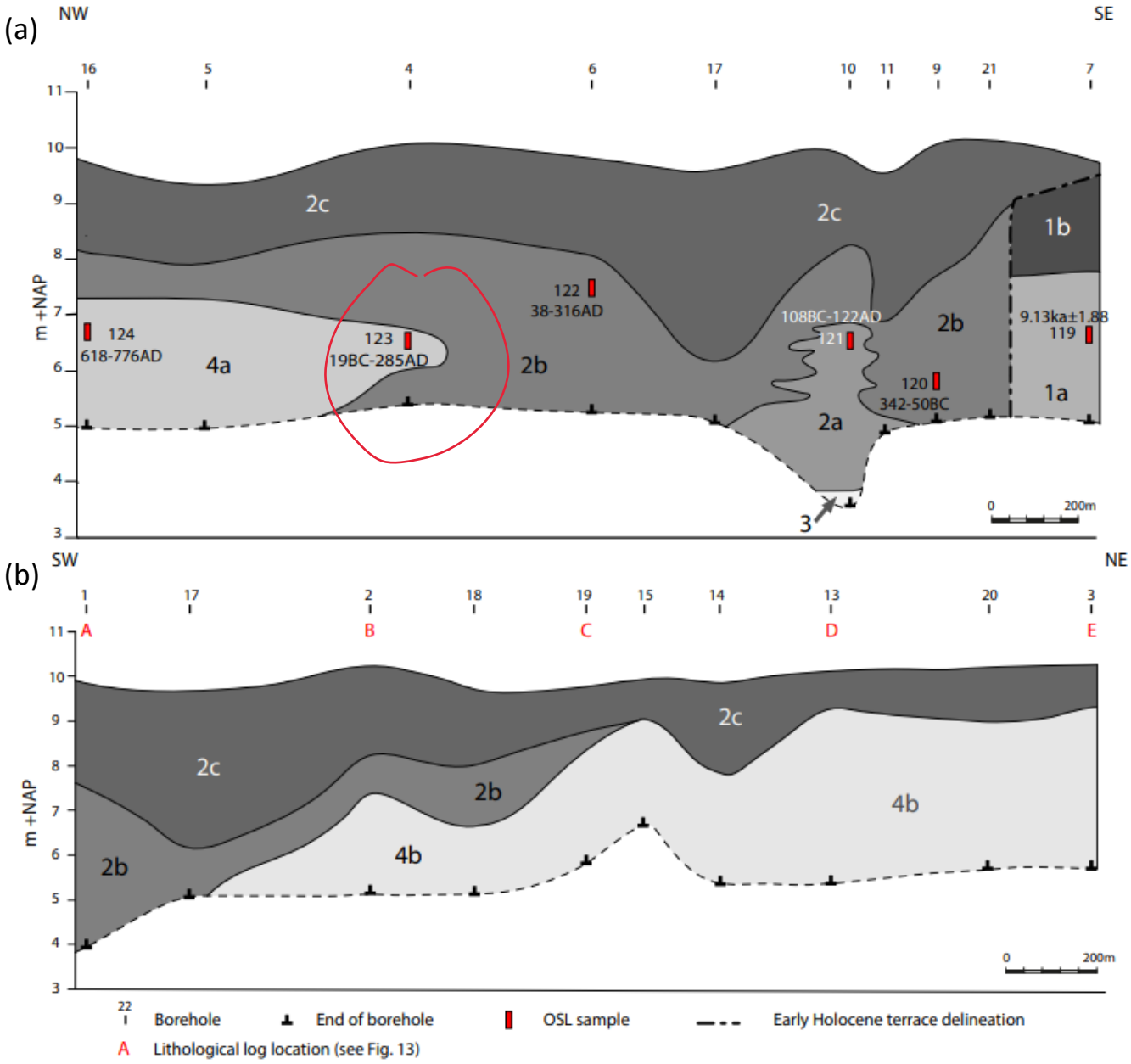

Figure 8: (a) Distribution of the identified facies in cross-section A (numbered; refer to Table 2 for descriptions). OSL sample locations are given with their abbreviated numbers (all preceded by NCL2321) and with the obtained ages; (b) Distribution of the identified facies in cross-section B (numbered; refer to Table 2 for descriptions), and locations of lithological logs shown in Fig. 13.

within their 10cm interval grain size classification. Facies 1a is topped by Facies 1b: a thick (±2m) layer of non-calcareous heavy clay.

Facies 2 is volumetrically the most significant facies in cross-section A (Fig. 8a) and consists predominantly of fine material. It has been subdivided into categories a, b and c based on lithology and distinguishing characteristics. Facies 2a is a well-sorted, fine-medium (150-300µm) narrow body of sand at the base of cross-section A, resting directly on top of Facies 3 (Fig 8a; Fig. 9b). Facies 2a is calcareous and contains some plant material throughout the base of the sequence. Surrounding Facies 2a and making up (most) of the lower depths of cross-section A is Facies 2b, consisting of silty and sandy clays with frequent occurrences of thin (<3cm) sand layers (Fig. 9a) and sporadic

Table 2: Descriptions and interpretations of the identified facies.

Facies		Lithology	Interpretation/ lithogenesis
1	a	Poorly sorted non-calcareous medium-coarse sands (210-1000 µm) with a well-developed fining upward sequence.	Early-Holocene terrace deposits
	b	Non-calcareous heavy clay.	Pre-Roman overbank deposits
2	a	Fine-medium well-sorted calcareous sands (150-300 µm).	Counterpoint deposits
	b	Clay and silty/sandy clays with distinct bands of fine to medium sands throughout.	Counterpoint deposits
	c	Homogenous heavy clays, light clays and sandy clays.	Counterpoint deposits/ overbank deposits
3		Well-rounded gravels up to 1cm diameter.	Channel-lag
4	a	Medium to coarse calcareous sands (210-2000 µm) with occasional gravel layers. No plant material.	Lower (downstream) point bar deposits
	b	Fine to coarse sands (150-2000 µm), gravelly in places. Distinct layers of plant material, clay layers and mud clasts.	Upper (upstream) point bar deposits

occurrences of slightly larger sand bodies (75-420µm) throughout. Facies 2b is calcareous and contains some plant material. This facies is also present at the base of cross section B (Fig. 8b) as a thick (±3m) sequence of material in the SW, gradually thinning and phasing out towards the centre of the cross-section. The fine material making up the upper 1-3m of sediments in cross-sections A and B belong to Facies 2c. This facies is characterised by homogenous heavy clays, silty clays or sandy clays, which may be slightly humic and can contain plant material. Facies 2c is variably calcareous, with the boreholes that contain more heavy clays often being less calcareous or non-calcareous (Appendix 1).

Facies 3 is only encountered once and consists of fine (5-16mm) well-rounded gravels found at 6-6.3m depth in borehole 10. This facies directly underlies Facies 2a, with a sharp transition from fine sand to gravel being observed (Fig. 9b).

Figure 9: Field photographs of defining characteristics of the identified facies: (a) Sand layers in clayey matrix typical of Facies 2b at 3.8m depth in borehole 9; (b) Gravel (Facies 3) encountered at 6m depth in borehole 10, overlain by fine sand of Facies 2a; (c) Gravel layers in Facies 4a at 4-4.4m depth in borehole 5; (d) Layer of plant material typical of Facies 4b in borehole 13 at 3.5-3.7m depth.

Facies 4 is present in both cross-sections and has been subdivided into Facies 4a and 4b. Facies 4a consists of medium to coarse (210-2000µm) calcareous sands which lack plant material. Gravelly sand and gravel layers occur frequently (Fig. 9c). This facies occurs at the base of the most NW boreholes (16 and 5) of Transect A (Fig. 8a) and is up to 2.4m thick. Facies 4b is volumetrically the most significant facies found in cross-section B as a several-metres-thick sequence at the base of the cross-section in the NE, gradually thinning out as Facies 2 overlying this sequence thickens towards the SW (Fig. 8b). It is a predominantly sandy facies varying from fine to coarse grained (150-2000µm), sporadically containing up to 25% gravel. Clay layers, mud clasts and distinct layers of plant material are characteristic of this facies (Fig. 9d).

4.2. OSL results

OSL results calculated using a bs-MAM are presented in Table 3 and shown on a map of the study area in Fig. 10. Despite the expectation that poor bleaching may have affected burial dose estimates, samples appeared to be overall well bleached, demonstrated by a lack of heterogenous De distributions and a general overlap of the age distributions within the MAM and CAM (Fig. 11). As expected, sample NCL2321-119 (borehole 7) is much older than the other samples, with an age of 9.13ka ± 1.88ka, confirming it does indeed fall within the early Holocene fluvial terrace (Mulder, 1989; Cohen et al., 2012; Willemse, 2019).

The remaining samples in Transect A date from 2.22 ± 0.15ka furthest from the present river to 1.32 ± 0.08ka closest to the present river (Fig. 10). This indicates the direction of sediment deposition to have taken place from the SE to the NW over time. Samples NCL2321-122 and NCL2321-123 are the only inconsistencies within this chronology with NCL2321-123 being slightly older despite being closer to the river; however, the proximity of the ages and overlapping error margins make the

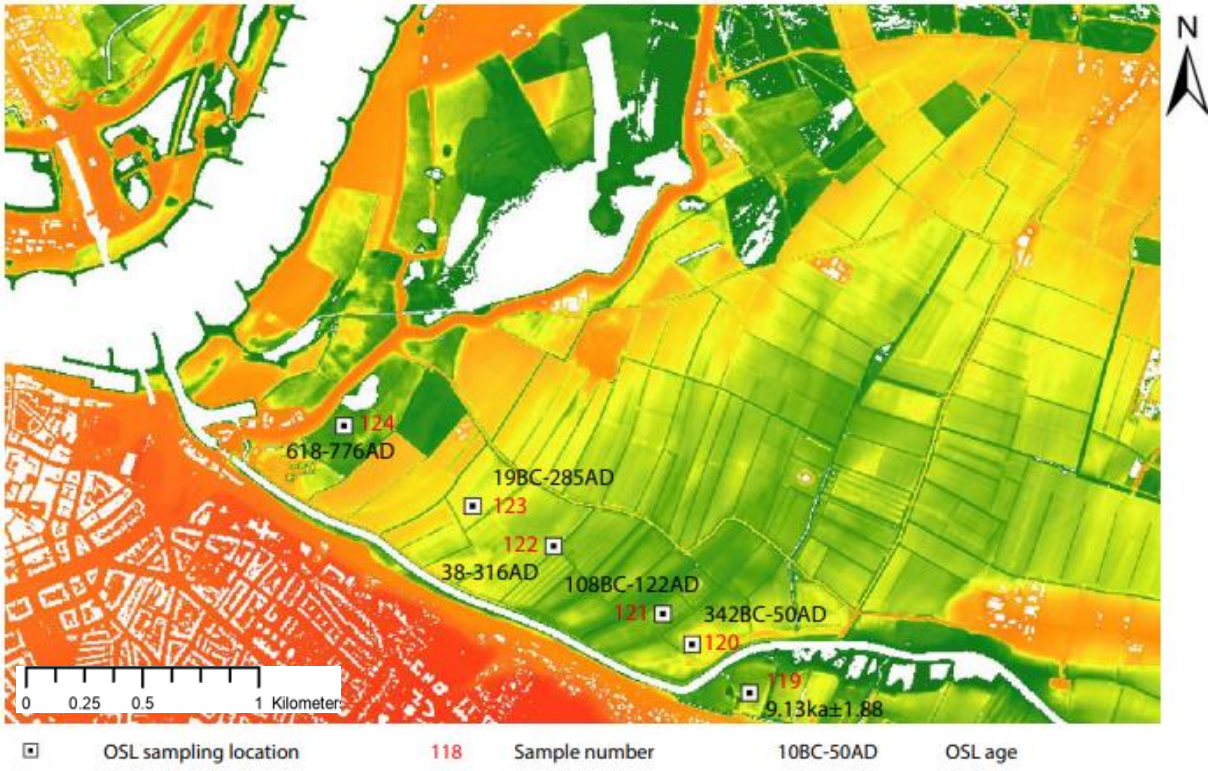

Figure 10: OSL sampling locations, abbreviated sample numbers (all preceded by NCL2321) and ages.

Table 3: OSL dating results. Locations shown on map in Fig. 10.

Sample	Coordinates (RD new)		Sample elevation (m +NAP)	OSL age (ka)		OSL age (BC - AD)
	x	y		μ	σ	
NCL2321-119	190619	427948	6.65	9.13	1.88	8988 BC – 5224 BC
NCL2321-120	190410	428124	5.73	2.22	0.15	342 BC- 50 BC
NCL2321-121	190304	428235	6.53	2.01	0.11	108 BC – 122 AD
NCL2321-122	189908	428481	7.53	1.84	0.14	38 - 316 AD
NCL2321-123	189614	428627	6.75	1.89	0.15	19 BC - 285 AD
NCL2321-124	428918	189146	6.44	1.32	0.08	618 – 776 AD

assumption that sediments become consistently younger towards the river a reasonable one given the remaining ages.

Based on these ages, the migration rate of the channel averaged 1.68m/year (calculated by dividing the distance between samples NCL2321-120 and NCL2321-124 by their modelled mean ages). Migration rates between samples NCL2321-120 and NCL2321-121 are notably slower than the average migration rate, calculated to be 0.72m/year.

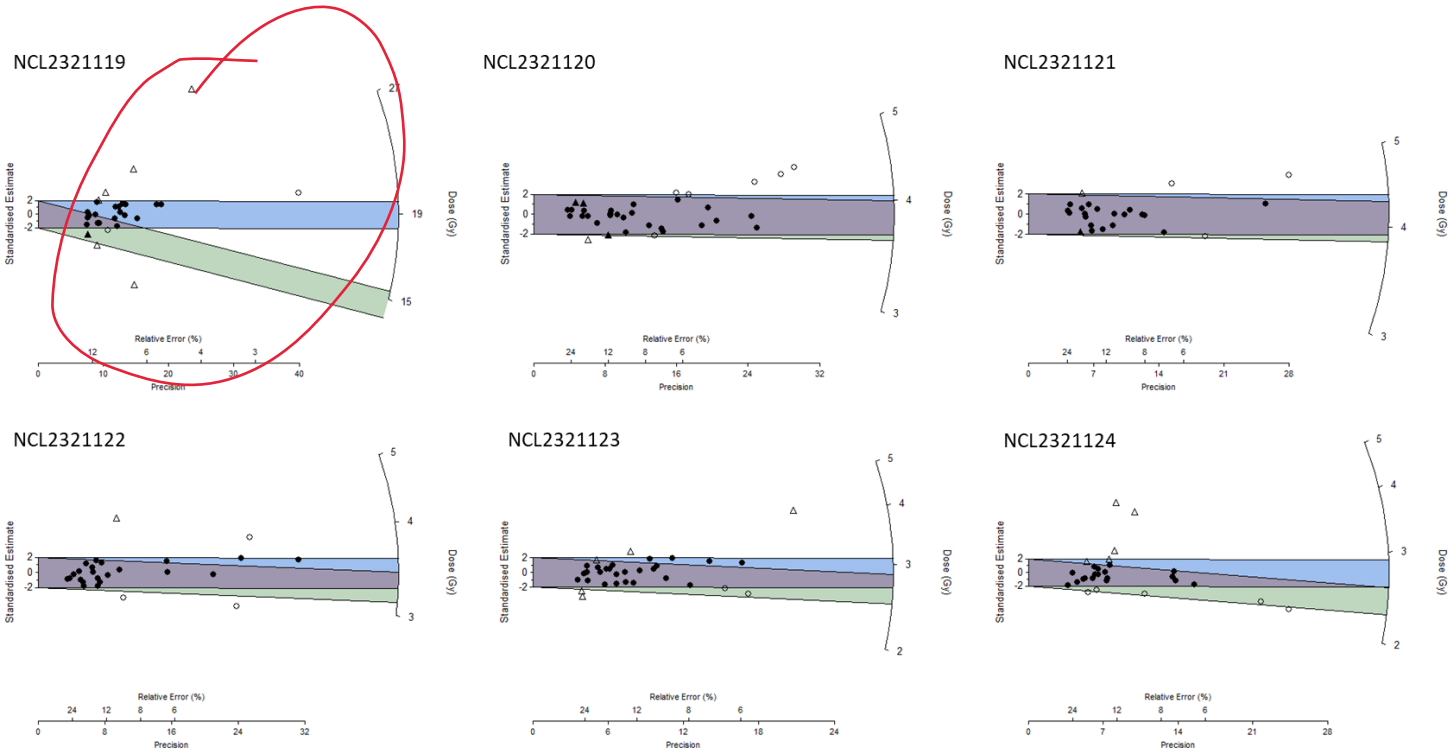

Figure 11: Radial plots showing the measured De distributions for each OSL sample. Filled circles fall within 2σ of the mean burial dose calculated by the central age model (blue shading). Green shading represents the 2σ range around the burial dose calculated by the minimum age model. Triangles represent outliers based on a calculation of the iterated mean burial dose using a 2σ threshold to determine whether a De measurement is rejected or not over six iterations.

4.3. GPR results

GPR measurements provided no useful results, with the signal depth of most profiles reaching only to ±1m. Because we expect the Roman-aged Waal to have a channel depth of around 6m (Willemse, 2019), profiles of this depth are of little relevance to processes associated with in-channel deposition. GPR transects 6 and 7, both perpendicular to the presumed counterpoint to point bar transition (Fig. 6b), consist of a somewhat clearer profile (Appendix 2), with signal depth up to 3m. Despite there appearing to be some potential lateral accretion surfaces in both profiles, these have a relatively small horizontal and vertical scale that thus can only questionably be related to such a large river system. It is more likely that these surfaces relate to accretion of sediments transported by water carried in the ditches where these profiles were made than that they are related to the river system. Additionally, uncertainty in the depth axis is introduced by the hyperbola fitting method (Sandmeier, 2020) since the electromagnetic velocity was derived from a different GPR transect due to lack of hyperbolas in these profiles. Because surface material may be heterogenous across the study area, the electromagnetic velocity may also show spatial heterogeneity and not be correct for this location. Given these uncertainties, the GPR profiles are not taken into account in the interpretation of the depositional process.

4.4. Data interpretation

The lithofacies identified in Section 4.1 have been interpreted in the context of the fluvial nature of the study area, taking into account the surrounding topography, surface morphology, chronology established by the OSL results and the relative positioning of the different facies within the two cross-sections. Fig. 12 shows a simplified map of our interpretation of the study area.

Facies 1a and 1b are identified as early-Holocene terrace deposits and pre-Roman overbank deposits respectively. The borehole in which this facies is identified (borehole 7) falls within the delineation of an early-Holocene terrace remnant east of the Ooij system (Fig. 4), with previous research confirming the presence of this river terrace (Mulder, 1989; Cohen & Stouthamer, 2012; Willemse, 2019). The boundary of the river terrace in cross-section A is estimated by using the waterway Het Meertje (Fig. 4) as delineation after Cohen & Stouthamer (2012). Despite their lithological differences, the heavy clay deposits of Facies 1a overlying the sandier terrace deposits of Facies 1b are drawn in Fig. 8a as part of the terrace given they were deposited as part of the Ressen river branch phase C system starting in the early Bronze age around 1800 BC (Willemse, 2019). This took place prior to the fluvial deposition of interest in this study during Roman times, and therefore these sediments are both classed into Facies 1 to distinguish older deposits from Roman-aged deposits, despite the large time period covered within this unit.

Facies 2, which forms most of cross-section A running parallel to the ice-pushed ridge, is interpreted as counterpoint deposits (Facies 2a, b, c), grading upward into overbank deposits (Facies 2c). The dominantly fine grained (Facies 2a) and clayey (Facies 2b, c) lithologies in found through much of the cross-section suggests a relatively low-energy depositional environment, with some variability which accounts for its non-homogeneity. This relatively fine texture indicates deposition likely to be sourced from suspension. The thickness of Facies 2 (up to 5m) excludes the possibility of this facies being comprised of solely overbank deposits when considering reconstructed channel geometries.

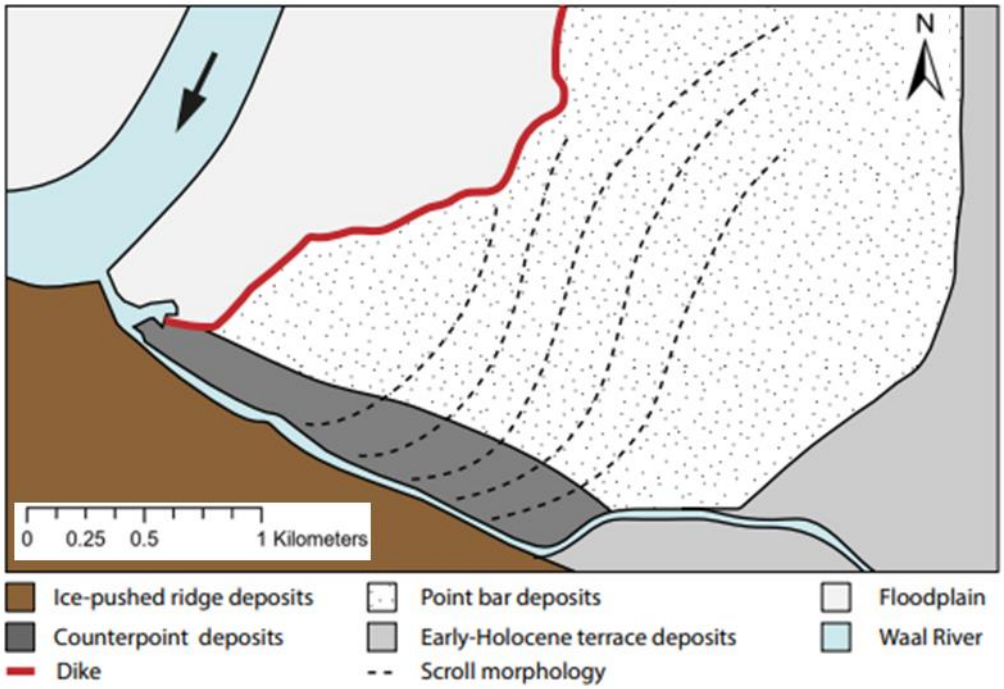

Figure 12: Simplified interpretation of deposits found in the study area.

Counterpoint deposits have been found to be potentially as thick as point bar deposits (Smith et al., 2009, 2011), which in our study area appears to also be the case given the stratigraphic relationship with Facies 3. The depth at which Facies 3 is located and its agreement with reconstructions of Roman-aged meander geometries that estimate the Waal to have been around 6m deep (Willemse, 2019), as well as the characteristic gravel lithology, leads to this facies being interpreted as channel lag. With Facies 2 directly overlying the channel lag, its thickness equals at least that of any associated point bar. Furthermore, sediments in Facies 2, particularly Facies 2b, concur with descriptions of counterpoint stratigraphy typically being clayey/silty, with occasional sand lenses comprising <20% of the total sedimentary unit (Smith et al., 2009). Despite Facies 2a being sandy, it is not uncommon for localised sand lenses to occur; for example Smith et al. (2011) found a sand to gross stratigraphy percentage of up to 45% in one of their cores of a counterpoint bar deposit in the Peace River, Alberta, Canada. Nanson & Croke (1992) describe counterpoint deposits as unique among floodplain deposits in that their deposition of fine sediments is a result of localised rather than overall low-energy environments. Such localisation can then also be expected to yield sediments that contain some heterogeneity in grain size, as we see in Facies 2a compared to the rest of Facies 2.

The surface morphology seen in the DEM further supports this interpretation, showing concave bends pointing upstream of the current location of the Waal (Fig. 4). These are in agreement with the typical orientation of those of counterpoint deposits, which arc in the upstream direction (Smith et al., 2009). Meanwhile, the OSL results indicate a SE-NW direction of accretion, with older sediments being found farther from the river, as would be expected for counterpoint deposition given that migration takes place in a downstream direction. These findings exclude the possibility of point bar formation followed by channel cut-off having taken place because for that scenario we would expect the chronology to be reversed.

Facies 4a, in the NW of cross-section A, underlying Facies 2, is comprised of coarser sands and gravel layers, and is interpreted as lower (downstream) point bar deposits. Relative to the ice-pushed ridge, the NW end of cross-section A is further away than the SE end (360m and 175m respectively). The associated counterpoint deposits in cross-section A that lie above Facies 4a are located slightly further upriver and closer to the inflection point than they are in the SE part of the cross section. Therefore they could be expected to be thinner (e.g. Fig. 13) than where the river reaches maximum curvature, i.e. closer to the ice-pushed ridge. Smith et al. (2009) found a similar trend in their studies of the Peace River where several profiles were made across each counterpoint bar, with those profiles closer to the inflection point showing thinner layers of silty counterpoint deposits. This would indicate that Facies 4a consists of the downstream end of the point bar lying adjacent to the counterpoint deposits directly beneath the ice-pushed ridge. Chronologically this agrees with our OSL findings, since accretion in the associated point bar would take place in the same direction as that of the counterpoint bar, just farther upstream.

Facies 4b is also interpreted as point bar deposits, complementing Facies 2 in cross-section B through their gradual transition across the profile that is typical for point bar-counterpoint bar boundaries (Sylvester et al., 2021). This can be seen in the lithological logs of several boreholes across Transect B, where sandy sediments of Facies 4b dominate the profile in the NE farthest from the ice-pushed ridge, with Facies 2 becoming dominant to the SW (Fig. 14). The composition of Facies 4b, being sandy with occasional gravel, silt/clay and plant material layers, matches descriptions of a wide range of point bar deposits globally (Allen, 1965). Its stratigraphic relationship with Facies 2 and the S-shaped surface morphology is typical of point bar deposits grading into counterpoint deposits (see Durkin et al., 2020; Makaske & Weerts, 2005; Smith et al., 2009, 2011; Fig. 2). Facies 2c is the only component of Facies 2 extending all the way across cross-section B, consisting solely of fine overbank deposits typically found on a point bar sequence in the NE half of the transect.

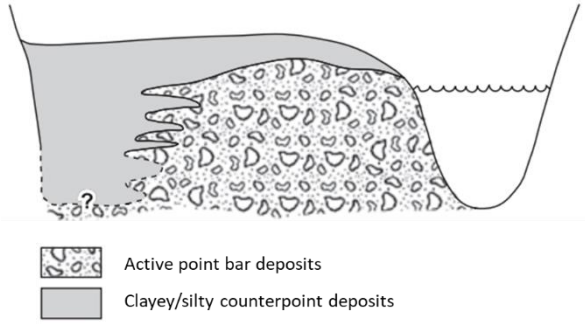

Figure 13: Hypothetical counterpoint-point bar transition showing thinning of clayey/silty deposits towards the inflection point. Source: Makaske & Weerts (2005).

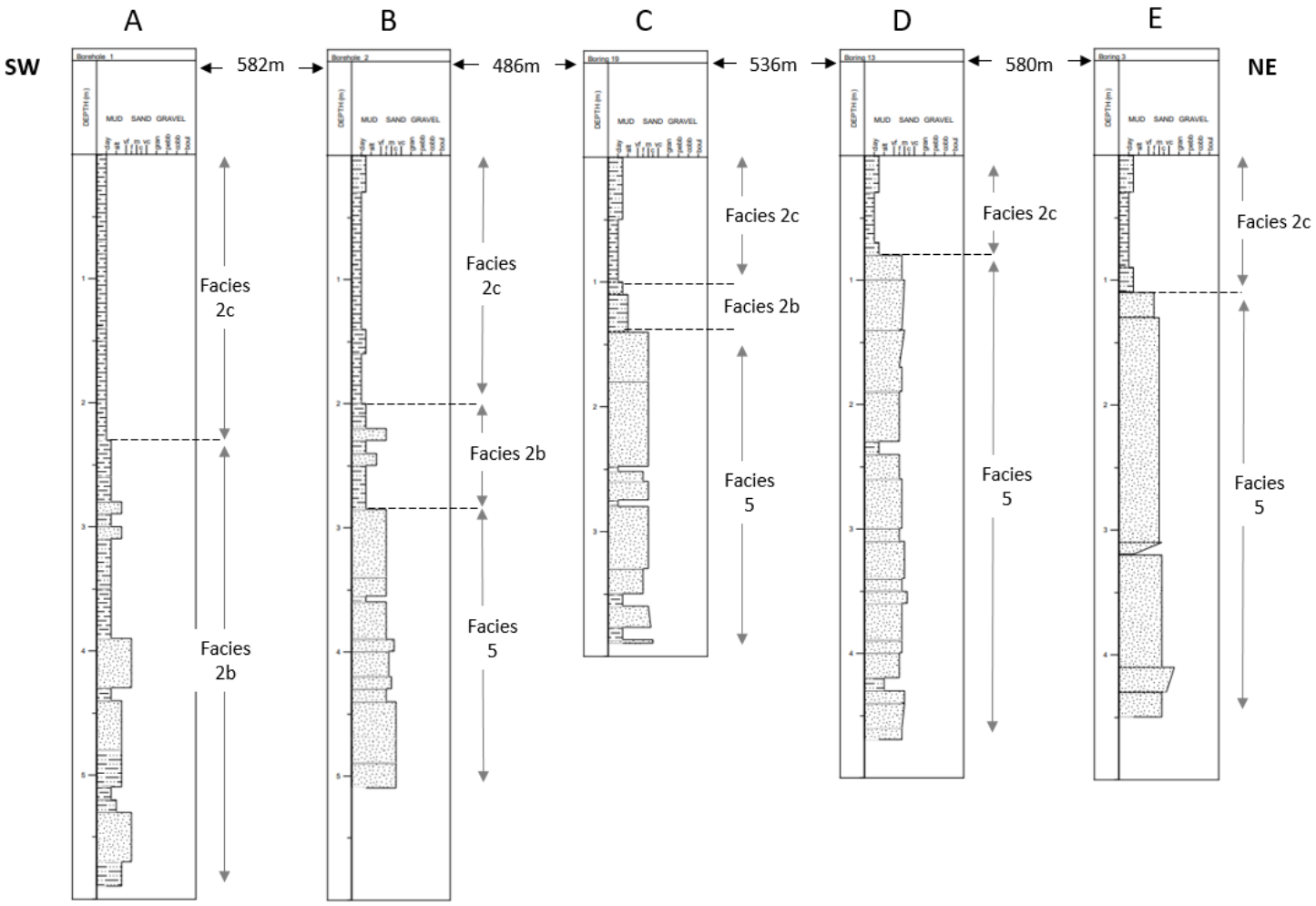

Figure 14: Sedimentary logs from boreholes in Transect B showing the transition from counterpoint bar deposits (SW) to point bar deposits (NE). For borehole locations refer to Figure 8b.

5. Discussion

5.1. Counterpoint depositional mechanisms

Despite having established that counterpoint deposits are present in the study area, some uncertainty still exists concerning the mechanism of deposition. While it has been postulated that counterpoint deposition can occur without a confined floodplain or non-erodible material in the outer bank of the river (Sylvester et al., 2021), the ice-pushed ridge in the study area and the resulting sharp bend attests to the presence of non-erodible material being a crucial factor in this case in facilitating counterpoint deposition.

Several mechanisms of counterpoint deposition have been described, which are summarised in three distinct processes as follows: (1) Makaske & Weerts (2005) and Smith et al. (2009) both describe that in bends meeting erosion resistant material at angles close to or greater than 90˚, the reverse flow resulting from this high angle impingement scours into the outer bank and forms a deep pool. This pool is then filled by a thick sequence of (fine) sand with a higher silt content distinguishing it from point bar deposits, called an eddy accretion deposit; (2) Page & Nanson (1982) describe flow expansion and separation taking place following deflection of the flow around the upstream point

bar, causing erosion of the opposite convex bank and resulting in widening of the bend. In this scenario, the availability of sufficient suspended material compared to bedload is necessary for infilling of the outer part bend and for restricting point bar formation in the downstream convex bank (Makaske & Weerts, 2005); (3) Counterpoint deposition can also be related to the weakening of secondary currents downstream of point bars, where a slack water zone develops (Nanson, 1980). This results in diffusion of suspended sediment towards, and deposition near, the concave bank (Makaske & Weerts, 2005).

Given the variability encountered within the counterpoint deposits identified in this study, it is difficult to attribute just one mechanism of deposition to their formation. Mechanism 1, where a scoured pool is filled by sandy eddy accretion deposits, could be associated with Facies 2a (borehole 10) identified in this study to explain the relatively sandy lithology present compared to the other subdivisions of Facies 2 (Fig. 8a; Table 2). Its relationship with the channel lag identified in Facies 3 could also speak for this mechanism of deposition. However, eddy accretion deposits have been described to be very thick as a result of deep scouring, and can be up to twice as thick as adjacent point bar deposits (Smith et al., 2009), which in our study area cannot be verified because channel lag was only encountered in one location. Furthermore, the angle at which the river met the ice-pushed ridge is notably less than the near- 90° where eddy accretion deposits form, as described by Makaske & Weerts (2005) and Smith et al. (2009). This angle is difficult to identify with certainty from only the surface morphology, especially given the agricultural land use and thus presumed modification of the landscape. However, it appears to have remained relatively consistent across the length of the counterpoint deposition zone based on the scroll bar morphology, and is estimated to be between 50-60° (Fig. 4; Fig. 12). Conversely, Smith et al. (2011) suggested eddy accretion deposits form at angles between 40-140° which does encompass the deposits identified in this study.

Mechanism 2, facilitated by flow expansion causing recirculation of flow in the outer bend of the river, could plausibly explain some of the variation seen in the study area. Page & Nanson (1982) described the forming of benches in the outer bend by secondary currents, comprised of basal medium to fine sands and topped with much finer deposits containing silts, clays and organics. This description also matches the lithologies identified in borehole 10 (Facies 2a overlain by Facies 2b and c; Fig. 8a), where Facies 2a could represent a bench formation. However, the lack of other 'benches' within the identified counterpoint deposits cause this explanation to be problematic, especially given their concave surface morphology that is relatively consistent. With the angle of impingement of flow not changing significantly across the counterpoint deposits, other factors must account for their variability. Changes in sediment supply or discharge could potentially also account for this, for example by human influence upstream of the study area (see also Section 5.5).

Diffusion of sediments towards the outer bank of the river by mechanism 3 could be related to Facies 2c identified in the study area, which consists of fine, homogenous heavy to light clays. Again however, this mechanism cannot be attributed to the entire length of identified counterpoint deposits, since the depth at which Facies 2c is present is not consistent across the transect (with the shallower depths consisting of overbank deposits). Based on observations in this study, and in other studies where various settings, depositional mechanisms and sedimentary products exist (Makaske &

Weerts, 2005; Page & Nanson, 1982; Smith et al., 2009, 2011; Sylvester et al., 2019), variability could be considered an inherent characteristic of counterpoint deposits. Indeed (Nanson & Croke, 1992) emphasise that counterpoint deposition takes place due to localised, rather than overall low-energy conditions, suggesting that different products of this deposition are also likely to be found locally rather than as large, homogenous units. In any case, the limited number of comparable studies in terms of fluvial systems, setting, time period and human influence make defining a single mechanism of counterpoint deposition for this study a considerable challenge. Establishing a wider knowledge base of the various products and mechanisms of counterpoint deposition across different settings is therefore required to further our understanding of these deposits.

5.2. OSL methodology and results

It can be argued that using the OSL method for dating fluvial sediments is unsuitable given the assumption that the luminescence signal has been reset before deposition (Wallinga, 2002). Small aliquots were used to measure De under the rationale that this would enable us to identify heterogenous bleaching within a sample should there be a lot of scatter in the De measurements, as larger aliquots tend to average a heterogenous De distribution (Wallinga, 2002). In our samples, clearly heterogenous distributions were not present (Fig. 11), which points to the samples being relatively well bleached, and thus giving a representative estimate of burial dose. A MAM (minimum age model) was still applied given the poor bleaching expected in a fluvial deposition environment. One of the sources of discussion on the use of such models is the sensitivity of the burial dose to the lowest De values and which degree of spread in the data is considered part of the burial dose population (Cunningham & Wallinga, 2012). Our radial plots, however, showed very little difference between the CAM and MAM for the younger samples (Fig. 11), suggesting minimal sensitivity of the calculated burial dose to the lower De values.

The overdispersion values calculated by the CAM also point to our samples being relatively well bleached and therefore minimising uncertainty for the dating method used. Cunningham et al. (2011) found that for small aliquots using a 2mm mask size, overdispersion on De for the CAM was 13.4% ± 2.2%. Samples NCL2321-120-123 show similar or lower overdispersion values (Table 4), considering we used a larger grain size (212-250µm compared to 180-200µm), which increases overdispersion of a sample (Cunningham et al., 2011; Cunningham & Wallinga, 2012). Higher overdispersion values for samples NCL2321-119 and NCL2321-124 can be attributed to the more extreme outliers in their De distributions (Fig. 11). Because we don't see evidence of distinct heterogenous De distributions for these samples, we can still assume the calculated burial doses are representative of actual ages. Sample NCL2321-119, which falls within the early Holocene terrace remnant, is the only sample for which the CAM appears to be a better fit than the MAM. However because this sample was taken only to provide a delineation of the study area, the use of a MAM here has little impact on our results concerning events during Roman times, despite the

Table 4: Overdispersion of the De estimate by the CAM.

Sample	Overdispersion CAM (%)
NCL2321119	0.26 ± 0.06
NCL2321120	0.08 ± 0.02
NCL2321121	0.07 ± 0.03
NCL2321122	0.17 ± 0.06
NCL2321123	0.16 ± 0.04
NCL2321124	0.32 ± 0.09

age of this sample likely being underestimated by the MAM.

The fact that OSL samples in this study were relatively well-bleached is unusual compared to other studies dating fluvial sediments (e.g. Quik & Wallinga, (2018)). This could be attributed to sediments being transported a greater distance, enabling sufficient exposure to light before deposition (Wallinga, 2002). Deposition taking place in a lower-energy environment where counterpoint deposition takes place could also clarify this, since more turbid waters (such as in a typical outer bend) reduce light infiltration and prevent resetting of the OSL signal (Wallinga, 2002; Quik & Wallinga, 2018). Additionally, deposition likely being sourced from suspended sediment rather than bedload may also contribute to the well-bleached nature of the sampled sediments.

5.3. Constraining channel locations

The paleogeographic reconstruction of the meander bend within the Ooijpolder is largely centred on the scroll morphology in the south of the study area at the foot of the ice-pushed ridge. Where previous interpretations focus on a paleochannel, here it is interpreted as a succession of NW-migrating counterpoint bars. Our interpretation stems from the types of sediments encountered in our borehole transects and their stratigraphical relationships, as well as their chronology. The borehole site locations however were limited to where access was possible regarding crop cycles (since the study area consists of agricultural land), and where permission was given by landowners to conduct the research. Based on our findings and on the multiple existing interpretations for evolution of this meander, we suggest that setting a borehole transect following the scroll morphology across the inflection point would give better and more consistent insight into the counterpoint-point bar transition. This would, in combination with additional OSL dates taken within the identified point bar, help to constrain channel position upstream of the counterpoint bars and enable this to be related to the evolution of the system at a larger scale. Similarly, a more consistent approach to borehole locations within Transect A relative to the surface morphology, for example more specifically targeting ridges and swales, could provide better insight into counterpoint bar variability and the surface morphology they produce. Especially with the considerable variability present in the identified counterpoint lithologies, relating this to the surface morphology could improve our understanding of these deposits.

In this study, the focus was centred on the evolution of the Roman-aged meander bend located in the Ooijpolder, however, this is of course part of a much larger system whose development beyond our study area may also yield further insights. Combining our own data with data from other studies on channel evolution upstream and downstream of our study location (e.g. Cohen et al., 2012; Heunks & van Hemmen, 2016; Willemse, 2019) can help to improve (and in some cases perhaps revise) paleogeographic reconstructions of the evolution of the fluvial system. The occurrence of localised channel processes such as counterpoint deposition in the Waal river, however, also carries the implication that such processes may have taken, or are currently, taking place in other parts of the Rhine-Meuse delta. As well as affecting paleogeographic reconstructions and our fundamental understanding of fluvial systems in the Netherlands, the occurrence of counterpoint deposition also has implications for river restorations projects and spatial planning. Indeed Kleinhans et al. (in press) recognised that the potential for habitats for aquatic species in stagnant zones of sharp bends is

often ignored in stream restoration practices. In order for restorations to be successful rather than requiring further management and perturbations to the natural system, it is essential that localised processes such as counterpoint deposition are accounted for in our spatial planning to enable prediction of the evolution of the system following restoration.

5.4. Alternative paleogeographic interpretations

As mentioned in Section 2.3, multiple paleogeographic interpretations of the study area exist, the most extensive of which are those of Willemse (2019) and Heunks & van de Geer (2021). These alternative interpretations will be compared and discussed in the context of the findings of this study.

Willemse (2019) interpreted the scroll bar morphology in which boreholes 10 and 11 (Fig. 6a) are located as a paleochannel that was cut off. However, this interpretation does not hold when looking at our OSL results, which show older samples farthest from the river, with sample age becoming progressively younger towards the river. In the scenario where the surface morphology does indeed represent a paleochannel, we would expect to find the chronology reversed, with lateral migration of this meander bend and point bar formation in a SE direction away from the present river. A ^{14}C date taken by the RGD in the same depression/scroll around 1km to the NE of our boreholes yields a date of 131-260 AD, taken at 7.88m +NAP, and is said to represent a late stage of channel filling. Our OSL dates for this same scroll closer to the ice-pushed ridge yield an age of 108 BC-122 AD (sample NCL2321-121), taken at 6.53m +NAP. Based on this study's interpretation (Fig. 12), the RGD ^{14}C date falls within a point bar complex formed by the channel migrating towards the present Waal location upstream of the counterpoint deposits at the foot of the ice-pushed ridge. In this scenario, the slightly younger age compared to sample NCL2321-121 could be explained by the sample being taken at a shallower depth, although the difference in ages is minimal considering the distance between the two samples.

The interpretation that a paleochannel lies in the Ooijpolder at the height of borehole 10 and the RGD ^{14}C date can further be disputed by the sediments identified in our boreholes. Assuming cut-off of the channel between 1-50 AD as shown in the paleogeographic reconstruction by Willemse (2019; Fig. 15), the mechanism of meander cut-off would be neck cut-off, resulting in formation of an oxbow that is filled by overbank flows (Allen, 1965). These sediments would be expected to consist of clays and silty clays since they are not in proximity to where the active channel supposedly lay after cut-off, whereas any fine to coarse sand bodies would be expected to be found at the upstream end of the channel fill sediments (Allen, 1965). Our boreholes in Transect A at the location of this presumed paleochannel show a thick fine sand succession in borehole 10 (Facies 2a), and adjacent clays with intermittent sand layers (Facies 2b), which are not typical of flood basin deposits, nor are they located at the upstream end of the supposed channel fill near to where the neck cut-off is assumed to have occurred.

The channel migration rate derived from OSL dates from this study are somewhat comparable to those of Willemse (2019), who, based on a remnant channel downstream of the study area west of Lent, calculated a migration rate of 1.8-2.6m per year. In this study, an average migration rate of

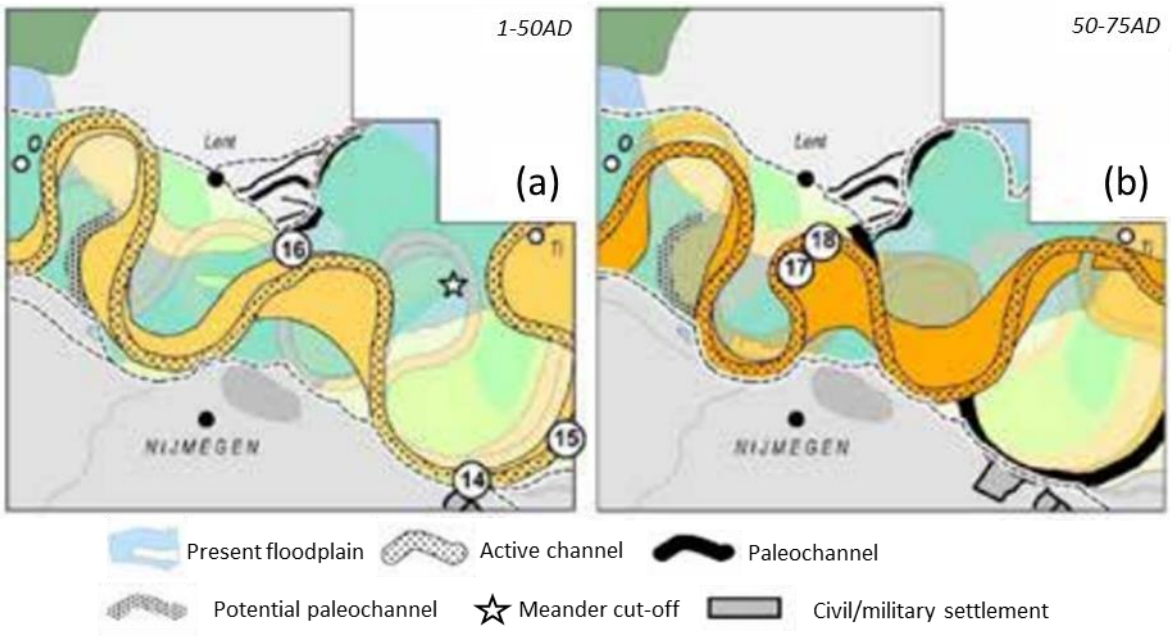

Figure 15: Evolutionary model of meanders in the Waal river between 1 and 75AD by Willemse (2019). (a) shows the presumed location where neck cut-off of the meander bend occurred, with (b) showing the paleochannel resulting from this neck cut-off.

1.68m/year was calculated, with minimum and maximum migration rates calculated based on OSL error margins to be 1.34-2.64m per year. However, little can be said on how rates of deposition between counterpoint bars and point bars compare given the different ages of meander bends, dating methods and locations. It could be expected that these rates may vary given the limited floodplain width caused by erosion resistant material in the outer bank at the site of counterpoint deposition, and based on sediment load composition of the river (ratio of suspended load to bedload).

The data obtained by Heunks & van de Geer (2021; see Section 2.3) also fit our own interpretation of counterpoint deposition having taken place. The older paleochannel abandoned by chute cut-off identified in their interpretation is described as being difficult to recognise within their borehole transect B (see Fig. 4 for transect locations), with their interpretation describing a sandy channel fill at the location of this transect, becoming more clayey towards the SW where it crosses their borehole transect C. The sandy sediments encountered in their transect B along the Persingsestraat would by our interpretation be part of the upstream point bar, with the southernmost borehole in their transect C at the foot of the ice-pushed ridge concurring with our own description of a counterpoint deposits, rather than these collective sediments representing a channel fill that is sandier upstream. In a study by Toonen et al. (2012) where a channel abandoned by means of chute cut-off to the north of the Waal is investigated (Ressen system), it was found that the sedimentary characteristics of the channel fill were comparable across the entire length of the cut-off channel. These consisted mainly of laminated silty clays showing a fining upward sequence in both grain size and lamination thickness. In this study, at the presumed paleochannel location, the thick layer of fine sand identified in borehole 10 does not concur with the sediments observed by Toonen et al. (2012). Given both cases assume chute cut-off to have taken place, it seems unlikely that two channel fills in

close proximity from the same river system would show such different sedimentary characteristics in their longitudinal profile.

Furthermore, our OSL results point to the direction of accretion of sediments beneath the ice-pushed ridge going towards the present river. Heunks & van de Geer (2021) largely base their interpretation of a second phase of meander expansion cut-off around 500 AD on a series of ^{14}C dates in the middle of the study area that are younger than those further to the SE (Fig. 16) within their first phase of meander cut-off (see Fig. 4 for channel locations). This second paleochannel was not identified in their borehole descriptions, but by using borehole descriptions from the Utrecht University database (Cohen, 2017) is hypothesized to have been located about 500m to the NW of their first phase meander cut-off location. However, our OSL dates indicate one clear accretion direction within the sediments at the foot of the ice-pushed ridge. Especially the youngest sample NCL2321-124 (closest to the present river) rules out the possibility of a second phase of meander expansion, given that for this scenario we would expect these sediments to be older than those further to the SE.

In general, our OSL results are comparable with the ^{14}C results from Heunks & van de Geer (2021; Fig. 16). Near the base of our identified counterpoint bar, four ^{14}C dates were taken by Heunks & van de Geer (2021) in a borehole at the foot of the ice-pushed ridge in the same presumed paleochannel as where our sample NCL2321-121 was taken in, which dates to 108 BC-122 CE. The ^{14}C dates show general agreement with this date, although stratigraphically their chronology is not entirely correct, with their uppermost sample pre-dating the one two metres below it. This could point to reworked material being contained within the sample, and highlights one of the potential limitations of radiocarbon dating for fluvial sediments (Wallinga, 2002; Rittentour, 2008). Further NW, the ^{14}C

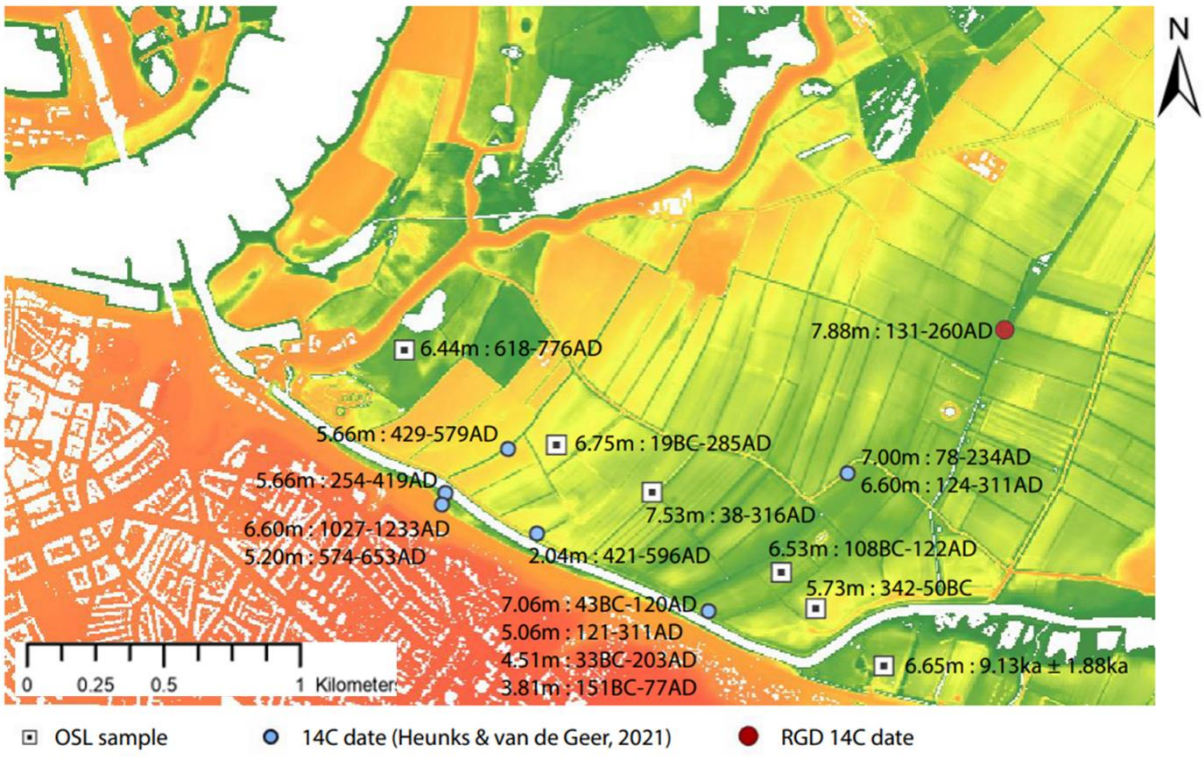

Figure 16: Digital elevation model of the study area showing ^{14}C dates and sample depths from previous studies, and OSL dates and sample depths from this study. From Heunks & van de Geer (2021) and De Jong (1983).

samples appear to yield similar ages or slightly younger than our own OSL samples within or near the same scroll morphology, although constraining the exact stratigraphic relationships across the different scroll bars and for differing depths of samples is difficult.

5.5. Archaeological context and human influence

Although there are abundant Roman-aged archaeological finds in Nijmegen, the location of a Roman-aged harbour remains unknown. A lack of continuous occupation at one site in Nijmegen during Roman presence (Driessen, 2007) has led to speculation that movement of the river resulted in a continuous relocation of settlements to more favourable locations (van den Broek et al., 2009; Daniel, 2016; Willemse, 2019). Whether our findings shed any light on the potential location of a Roman harbour is questionable given the error margins associated with the OSL ages obtained. At the time of initial Roman occupation in Nijmegen, based on our OSL dates the river channel within the Ooijpolder would have been located approximately between the Hunerberg and Kops Plateau military camps (Fig. 5) at the foot of the ice-pushed ridge around 7 AD (Sample NCL2321-121 in borehole 10; Fig. 6). Proximity to the river may have played a role in the initial location of these camps, although this can also be attributed to the strategic location topographically, being located in the highest part of the landscape (Driessen, 2007). Previous excavations here at the base of the ice-pushed ridge by Daniel (2016; Fig. 4), however, did not yield any evidence of a Roman harbour.

Later stages of Roman civilian settlement at Valkhof are topographically better situated for access to the river during the stages of Roman settlement from 70 AD onwards, although channel migration rates may have been slightly faster in this part of the study area compared to the average. Just prior to Roman occupation, channel migration took place at rate of 0.72m/year between OSL samples NCL2321-120 and NCL2321-121, compared to the average of 1.68m/year across the entire transect. Indeed, van den Broek et al. (2009) and Willems (1990) both mention the Roman settlements at Valkhof as a centre for trade and thus a potential harbour location. Driessen (2007), on the other hand, points out *Ulpia Noviomagus*, in the present Waterkwartier in Nijmegen-West, as a potential location for a civilian harbour. It is interesting to consider that the depositional environment in sharp bends where counterpoint deposits are found may be an ideal setting for a natural harbour; counterpoint zones are often low energy environments due to downstream rather than lateral migration, and/or are relatively deep due to scouring by reverse flows (Makaske & Weerts, 2005) . However, given the short time periods during which the Romans were active in Nijmegen and the by comparison large uncertainty of our OSL ages, it is difficult to draw sound conclusions as to the influence of the channel movement on Roman settlement location.

As already mentioned, studies of counterpoint deposition in the Netherlands are limited to those of Makaske & Weerts (2005) and Candel et al. (2020) where counterpoint deposits from the period 3800-3000 BP and 8.5-2.5ka were identified in the Hennisdijk channel belt and the Dommel system respectively. These systems developed in a period considered pre-human influence. The well-documented presence of the Romans in Nijmegen during counterpoint bar development at the foot of the ice-pushed ridge raises the question whether the associated deposits and channel migration were affected by human influence. Although the construction of dikes took place several centuries

after Roman occupation, there is evidence that the Romans modified the fluvial system in other ways.

Upstream of our study area near Lobith, a Roman dam was built around 12BC during their early occupation at the bifurcation of the Waal and the Nederrijn in attempt to make the latter more accessible for ships (Willems, 1986; van den Broek et al., 2009). This dam was removed in 70 AD after the Batavian revolt, though it is speculated to have been restored after a peace was reached (van den Broek et al., 2009). A reduction in discharge of the Waal with building of the dam and subsequent increase in discharge with its removal may have influenced the sediment load capacity of the river. It could be speculated that the lithological variation in cross-section A seen between Facies 2a (borehole 10, OSL sample NCL2321-121) and the adjacent-lying Facies 2b may have been impacted by this fluctuating discharge depositing the coarser sediments from Facies 2a during a period of increased discharge following destruction of the dam.

The question of the location of a Roman harbour also highlights a potential form of modification of the fluvial system at the time of counterpoint deposition. If the harbour was indeed located at the foot of the ice-pushed ridge, we may expect this to have impacted depositional processes. However, given the short and discontinuous periods of Roman settlement at various locations in Nijmegen, it is questionable whether this impact is visible in the sedimentary record. Findings of a Roman-aged millstone at the confluence of Het Meertje and the present Waal (van den Broek et al., 2009) also provide evidence of further channel modification, however this site is beyond our borehole transects that lie inside the present dikes.

The fact that the Romans in some way would have modified the fluvial system is clear. This may limit the validity of our sedimentological comparisons of the identified counterpoint deposits with those in natural systems (Makaske & Weerts, 2005; Smith et al., 2009, 2011). The uncertainty about the exact location of a Roman harbour makes it difficult to assess the impact of human influence on depositional processes. However, the role of human influence should be kept in mind when interpreting modern counterpoint deposits and, given the relative scarcity of studies on counterpoint deposition, is a topic that requires further research.

6. Conclusions

This study explored the potential for counterpoint deposition to have taken place in a Roman-aged sharply curved meander bend of the Waal River by Nijmegen. The research questions can be answered as follows:

1. The sediments found in the scroll bar morphology in the SW of the Ooijpolder consist of a thick sequence of fine, clay-dominated sediments that match descriptions of counterpoint deposits. These grade into sandier point bar deposits further upstream (to the NE).
2. The OSL ages obtained during this study indicate the direction of sediment accretion at the foot of the ice-pushed ridge, and thus the direction of channel movement, to be from the SE to the NW towards the present river. This means that the channel migrated in a downstream direction, as is the case for counterpoint deposits.

3. The internal structure and lateral accretion surfaces of the deposits in the study area were unable to be identified using GPR due to the prevalence of clayey sediments at the surface limiting signal depth. However, the direction of sediment accretion was able to be established by the OSL ages obtained.

The results of this study have implications for the paleogeographic reconstruction of the study area, as presently several different interpretations exist that do not involve counterpoint deposition. Recognition of modern counterpoint deposition in the fluvial record in the Netherlands is extremely relevant for the understanding of meandering channel processes which dominate Dutch fluvial systems. In the context of river and stream restoration practises which are becoming increasingly more common, as well as for spatial planning, the need for further research and an improved understanding counterpoint deposition is required in order for these restorations to be sustainable.

Several areas for further research have been highlighted by this study. Firstly, in the local context, our understanding of the identified counterpoint deposits, their dimensions, and their variability can be improved. Taking OSL samples in the upstream point bar can help to constrain the previous channel location and enable comparison of counterpoint and point bar accretion rates. Placing boreholes over the identified counterpoint deposits targeting the scrolls and swales can give better insight into counterpoint bar variability and their relationship with the surface morphology. Secondly, a broader knowledge base on counterpoint deposits forming in various settings, and their mechanisms of deposition, is required for sound conclusions concerning their formation to be drawn, which can then better inform restoration projects and spatial planning. Thirdly, a lack of knowledge on the extent of human influence on counterpoint depositional processes has been identified, with existing studies largely focusing on systems developed prior to human influence. Given the extent of river and stream management in present-day societies, it is crucial to close this knowledge gap for the successful management of our waterways.

References

Aitken, M. (1998). *Introduction to optical dating: the dating of Quaternary sediments by the use of photon-stimulated luminescence*. Clarendon Press, Oxford.

Allen, J. (1965). A review of the origin and characteristics of recent alluvial sediments. *Sedimentology*, *5*(2), 89–191.

Berendsen, H. J. A., & Stouthamer, E. (2000). Late Weichselian and Holocene palaeogeography of the Rhine-Meuse delta, the Netherlands. *Palaeogeography, Palaeoclimatology, Palaeoecology*, *161*(3–4), 311–335. https://doi.org/10.1016/S0031-0182(00)00073-0

Blanckaert, K. (2011). Hydrodynamic processes in sharp meander bends and their morphological implications. *Journal of Geophysical Research: Earth Surface*, *116*. https://doi.org/10.1029/2010JF001806

Brierley, G., & Fryirs, K. (2009). Don't fight the site: three geomorphic considerations in catchment-scale river rehabilitation planning. *Environmental Management*, *43*(6), 1201–1218. https://doi.org/10.1007/s00267-008-9266-4

Candel, J., Kleinhans, M., Makaske, B., & Wallinga, J. (2021). Predicting river channel pattern based on stream power, bed material and bank strength. *Progress in Physical Geography: Earth and Environment*, *45*(2), 253–278. https://doi.org/10.1177/0309133320948831

Candel, J., Makaske, B., Kijm, N., Kleinhans, M. G., Storms, J. E., & Wallinga, J. (2020). Self-constraining of low-energy rivers explains low channel mobility and tortuous planforms. *The Depositional Record*, *6*(3), 648–669. https://doi.org/10.1002/dep2.112

Chamberlain, E., Wallinga, J., & Shen, Z. (2018). Luminescence age modeling of variably-bleached sediment: Model selection and input. *Radiation Measurements*, *120*, 221–227.

Cohen, K. M., & Stouthamer, E. (2012). *Digitaal Basisbestand Paleogeografie van de Rijn-Maas Delta*. https://doi.org/https://doi.org/10.17026/dans-x7g-sjtw

Cohen, K. (2012). *LLG 2012 (Version 2.0.25) [computer programme]*. Utrecht University.

Cohen, K. (2017). *Laaglandgenese boringendatabase Universiteit Utrecht. DANS.* https://doi.org/https://doi.org/10.17026/dans-zcv-knya

Cohen, K, Stouthamer, E., Pierik, H., & Geurts, A. (2012). *Rhine-Meuse Delta Studies' Digital Basemap for Delta Evolution and Palaeogeography.* http://xn--persistentidentifier-ks2l.nl/?identifier=urn:nbn:nl:ui:13-nqjn-zl

Cohen, KM, & Stouthamer, E. (2012). *VERNIEUWD DIGITAAL BASISBESTAND PALEOGEOGRAFIE VAN DE RIJN-MAAS DELTA. Beknopte toelichting bij het Digitaal Basisbestand Paleogeografie van de Rijn- Maas Delta.* https://easy.dans.knaw.nl/ui/datasets/id/easy-dataset:52125

Cunningham, A., & Wallinga, J. (2010). Selection of integration time intervals for quartz OSL decay curves. *Quaternary Geochronology*, *5*(6), 657–666. https://www.sciencedirect.com/science/article/pii/S1871101410000610

Cunningham, A., & Wallinga, J. (2012). Realizing the potential of fluvial archives using robust OSL chronologies. *Quaternary Geochronology*, *12*, 98–106. https://www.sciencedirect.com/science/article/pii/S1871101412001069

Cunningham, A., Wallinga, J., & Minderhoud, P. (2011). Expectations of scatter in equivalent-dose distributions when using multi-grain aliquots for OSL dating. *Geochronometria*, *38*(4), 424–431. https://doi.org/10.2478/s13386-011-0048-z

Daniël, A. (2016). *Op zoek naar de Romeinse Haven bij Ubbergen*. Gemeente Nijmegen, Bureau Leefomgevingskwaliteit, Archaeologie.

De Bakker, H., & Schelling, J. (1966). Systeem van bodemclassificatie voor Nederland. De hogere niveaus. *Grondboor & Hamer*, *20*(5), 229.

Driessen, M. (2007). *Bouwen om te blijven. De topografie, bewoningscontinuïteit en monumentaliteit van Romeins Nijmegen*. Universiteit van Amsterdam, Amsterdam.

Durkin, P. R., Hubbard, S. M., Holbrook, J., Weleschuk, Z., Nesbit, P., Hugenholtz, C., Lyons, T., & Smith, D. G. (2020). Recognizing the product of concave-bank sedimentary processes in fluvial meander-belt strata. *Sedimentology*, *67*(6), 2819–2849. https://doi.org/10.1111/SED.12743

Galbraith, R., Roberts, R., Laslett, G., Yoshida, H., & Olley, M. (1999). Optical dating of single and multiple grains of quarts from Jinmium rock shelter, northern Australia: Part 1, experimental design and statistical models. *Archeometry*, *41*(2), 339–364.

Heunks, E., & van de Geer, P. (2021). *Landschappelijk booronderzoek Ooijpolder: een onderzoek naar de ligging en ouderdom van de restgeulen in het westelijke deel van de Ooijpolder, gemeente Berg en Dal*. Bureau Archeologie en Bodemkwaliteit gemeente Nijmegen, Nijmegen.

Heunks, E., & van Hemmen, F. (2016). *Archeologische monumentenzorg in het plan- gebied van de dijkteruglegging bij Lent. 3. In het krachtenspel van mens en Waal. Een biografie van het Lentse land*. Gemeente Nijmegen, Bureau Leefomgevingskwaliteit, Archeologie, Nijmegen.

Hobo, N., Makaske, B., Wallinga, J., & Middelkoop, H. (2014). Reconstruction of eroded and deposited sediment volumes of the embanked River Waal, the Netherlands, for the period ad 1631–present. *Earth Surface Processes and Landforms*, *39*(10), 1301–1318. https://doi.org/10.1002/esp.3525

Makaske, B., & Weerts, H. J. T. (2005). Muddy lateral accretion and low stream power in a sub-recent confined channel belt, Rhine-Meuse delta, central Netherlands. *Sedimentology*, *52*(3), 651–668. https://doi.org/10.1111/j.1365-3091.2005.00713.x

Mason, J., & Mohrig, D. (2019). Scroll bars are inner bank levees along meandering river bends. *Earth Surface Processes and Landforms*, *44*(13), 2649–2659.

Middelkoop, H., & Haselen, C. O. G. van. (1999). *Twice a river : Rhine and Meuse in the Netherlands*. RIZA report 99.003, isbn 9036952239. Ministry of transport, public works and water management, The Hague.

Mulder, J. (2008). *Bodemkundig onderzoek van het terrein HAVO Notre Dame des Anges te Beek-Ubbergen i.v.m. nieuwbouw*. Gemeente Ubbergen, Beek-Ubbergen.

Mulder, JR. (1989). *De bodemgesteldheid van het herinrichtingsgebied'Ooypolder'*. Stichting voor bodemkartering, Wageningen.

Murray, A., & Wintle, A. (2000). Luminescence dating of quartz using an improved single-aliquot regenerative-dose protocol. *Radiation Measurements*, *32*(1), 57–73. https://www.sciencedirect.com/science/article/pii/S135044879900253X

Nanson, G. (1980). Point bar and floodplain formation of the meandering Beatton River, northeastern British Columbia, Canada. *Sedimentology*, *27*(1), 3–29. https://doi.org/10.1111/J.1365-3091.1980.TB01155.X

Nanson, G., & Croke, J. (1992). A genetic classification of floodplains. *Geomorphology*, *4*(6), 469–486. https://www.sciencedirect.com/science/article/pii/0169555X9290039Q

Nanson, G., & Page, K. (1983). Lateral Accretion of Fine-Grained Concave Benches on Meandering Rivers. *Modern and Ancient Fluvial Systems*, 133–143. https://doi.org/10.1002/9781444303773.CH10

Nelson, M., & Rittenour, T. (2015). Using grain-size characteristics to model soil water content: Application to dose-rate calculation for luminescence dating. *Radiation Measurements*, *81*, 142–149. https://www.sciencedirect.com/science/article/pii/S1350448715000438

Page, K., & Nanson, G. (1982). Concave-bank benches and associated floodplain formation. *Earth Surface Processes and Landforms*, *7*(6), 529–543. https://doi.org/10.1002/ESP.3290070603

Prescott, J., & Hutton, J. (1994). Cosmic ray contributions to dose rates for luminescence and ESR dating: large depths and long-term time variations. *Radiation Measurements*, *23*(2–3), 497–500. https://www.sciencedirect.com/science/article/pii/1350448794900868

Preusser, F., Degering, D., Fuchs, M., Hilgers, A., Kadereit, A., Klasen, N., & Spencer, J. (2008). Luminescence dating: basics, methods and applications. *E&G Quaternary Science Journal*, *57*(1/2), 95–149. https://egqsj.copernicus.org/articles/57/95/2008/

Quik, C., & Wallinga, J. (2018). Reconstructing lateral migration rates in meandering systems–a novel Bayesian approach combining optically stimulated luminescence (OSL) dating and. *Earth Surface Dynamics*, *6*(3), 705–721. https://esurf.copernicus.org/articles/6/705/2018/

Rhodes, E. J. (2011). Optically stimulated luminescence dating of sediments over the past 200,000 years. *Annual Review of Earth and Planetary Sciences*, *39*, 461–488. https://doi.org/10.1146/ANNUREV-EARTH-040610-133425

Rittentour, T. (2008). Luminescence dating of fluvial deposits: applications to geomorphic, palaeoseismic and archaeological research. *Boreas*, *37*(4), 613–635. https://doi.org/10.1111/j.1502-3885.2008.00056.x

Sandmeier, K. (2020). *Windows™ XP/7/8/10-program for the processing of seismic, acoustic or electromagnetic reflection, refraction and transmission data*.Windows™, Karlsruhe.

Schnauder, I., & Sukhodolov, A. N. (2012). Flow in a tightly curving meander bend: effects of seasonal changes in aquatic macrophyte cover. *Earth Surface Processes and Landforms*, *37*(11), 1142–1157. https://doi.org/10.1002/esp.3234

Smith, D. G., Hubbard, S. M., Lavigne, J. R., Leckie, D. A., & Fustic, M. (2011). Stratigraphy of Counter-Point-Bar and Eddy-Accretion Deposits in Low-Energy Meander Belts of the Peace-Athabasca Delta, Northeast Alberta, Canada. *From River to Rock Record: The Preservation of Fluvial Sediments and Their Subsequent Interpretation: SEPM*, *Special Publ*(97), 143–152. https://doi.org/10.2110/sepmsp.097.143

Smith, D. G., Hubbard, S. M., Leckie, D. A., & Fustic, M. (2009). Counter point bar deposits: Lithofacies and reservoir significance in the meandering modern peace river and ancient McMurray formation, Alberta, Canada. *Sedimentology*, *56*(6), 1655–1669. https://doi.org/10.1111/j.1365-3091.2009.01050.x

Sylvester, Z., Durkin, P., & Covault, J. (2019). High curvatures drive river meandering. *Geology*, *47*(3), 263–266. https://pubs.geoscienceworld.org/gsa/geology/article-abstract/47/3/263/568705

Sylvester, Z., Durkin, P. R., Hubbard, S. M., & Mohrig, D. (2021). Autogenic translation and counter point bar deposition in meandering rivers. *GSA Bulletin*, 1–18. https://doi.org/10.1130/b35829.1

Thijssen, J., & Wildenberg, J. (2005). *Vondsten uit de klei. Een verkennend archeologisch onderzoek in het Circul van Ooij-gemeente Ubbergen.* Gemeente Nijmegen, Bureau Archeologie, Nijmegen. https://doi.org/10.17026/dans-xef-wfrc

Toonen, W., Kleinhans, M., & Cohen, K. (2012). Sedimentary architecture of abandoned channel fills. *Earth Surface Processes and Landforms*, *37*(4), 459–472. https://doi.org/10.1002/esp.3189

van den Broek, P., van Enckevort, H., & Thijssen, J. (2009). “De oeverbewoners noemen hem Vahalis”. De Waal bij Nijmegen in de Romeinse tijd. In *Jaarboek Numaga LVI* (pp. 15–31). Vereniging Numaga.

van der Heijden, P. (2016). *Grens van het Romeinse rijk. De limes in Gelderland.* Uitgeverij Matrijs.

Wallinga, J. (2002). Optically stimulated luminescence dating of fluvial deposits: a review. *Boreas*, *31*(4), 303–322. https://doi.org/10.1111/J.1502-3885.2002.TB01076.X

Wallinga, J., & Bos, I. (2009). Optical dating of fluvio-deltaic clastic lake-fill sediments-A feasibility study in the Holocene Rhine delta (western Netherlands). *Quaternary Geochronology*, *5*(5), 602–610. https://doi.org/10.1016/j.quageo.2009.11.001

Wallinga, J., Hobo, N., Cunningham, A., Versendaal, A., Makaske, B., & Middelkoop, H. (2010). Sedimentation rates on embanked floodplains determined through quartz optical dating. *Quaternary Geochronology*, *5*(2–3), 170–175.

Wallinga, J., & Van der Staay, J. (1999). Sampling in waterlogged sands with a simple hand-operated corer. *Ancient TL*, *17*(2), 59–61.

Willems, W. (1986). *Romans and Batavians A Regional Study in the Dutch Eastern River Area*. Universiteit van Amsterdam, Amsterdam.

Willems, W. (1990). *Romeins Nijmegen. Vier eeuwen stad en centrum aan de Waal*. Uitgeverij Matrijs, Utrecht. https://scholarlypublications.universiteitleiden.nl/access/item%3A2732103/view

Willemse, N. (2019). *De vroege Waal bij Nijmegen . Stratigrafie , sedimentologie en genese van laatholocene rivierafzettingen tussen Nijmegen en Lent*. RAAP- Rapport 3208. Gemeente Nijmegen, Nijmegen.

Wintle, A., & Murray, A. (2006). A review of quartz optically stimulated luminescence characteristics and their relevance in single-aliquot regeneration dating protocols. *Radiation Measurements*, *41*(4), 369–391.

Appendix 1: LLG borehole profiles

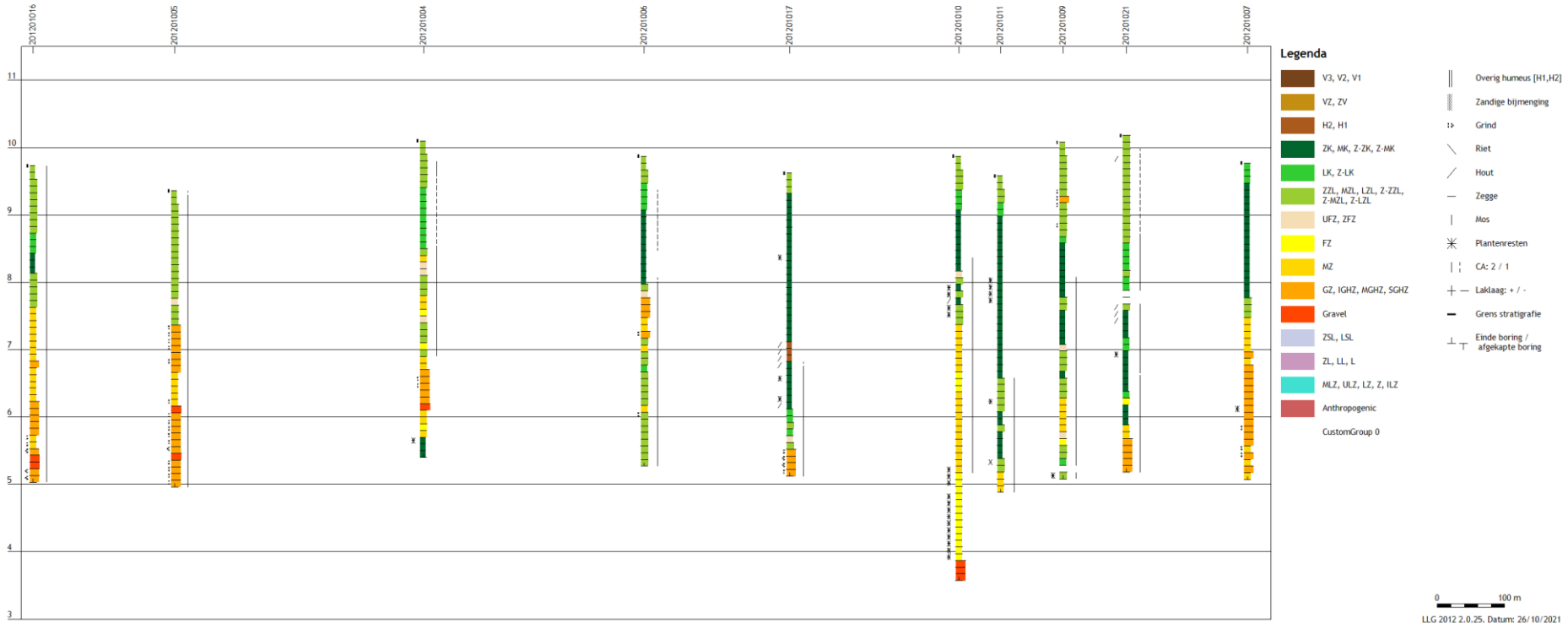

Transect A

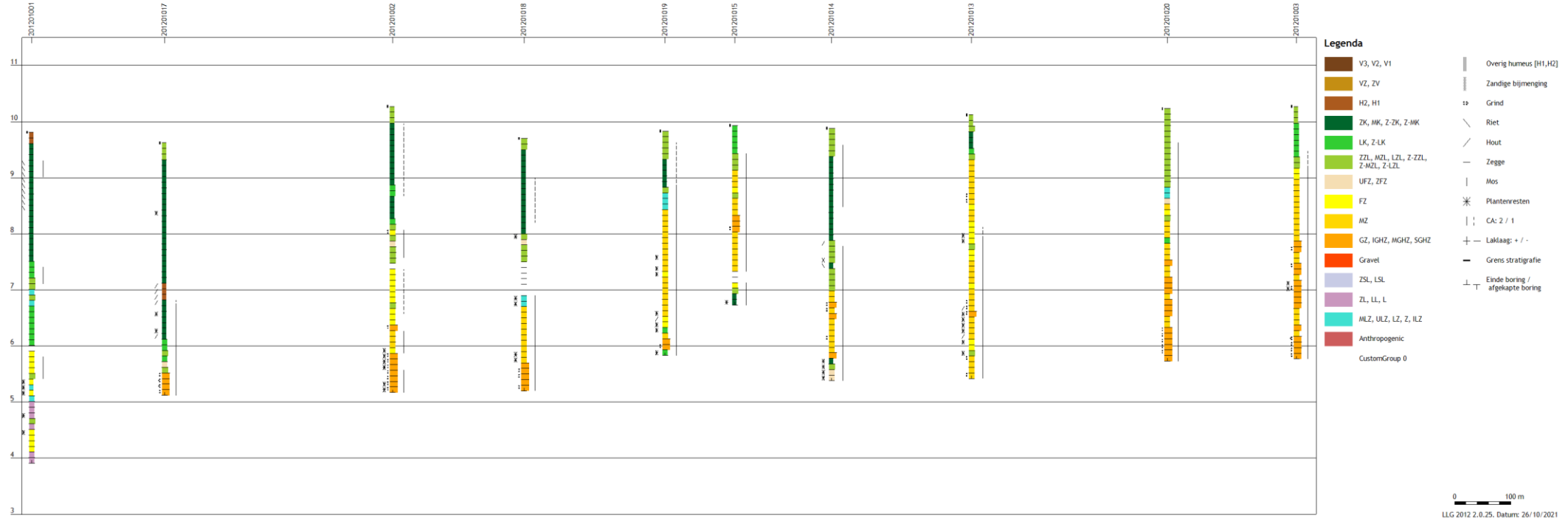
201201001
201201017
201201002
201201018
201201019
201201015
201201014
201201013
201201020
201201003
11
10
9
8
7
6
5
4
3
Legenda
V3, V2, V1
VZ, ZV
H2, H1
ZK, MK, Z-ZK, Z-MK
LK, Z-LK
ZZL, MZL, LZL, Z-ZZL, Z-MZL, Z-LZL
UFZ, ZFZ
FZ
MZ
GZ, IGHZ, MGHZ, SGHZ
Gravel
ZSL, LSL
ZL, LL, L
MLZ, ULZ, LZ, Z, ILZ
Anthropogenic
CustomGroup 0
Overig humeus [H1,H2]
Zandige bijmenging
Grind
Riet
Hout
Zegge
Mos
Plantenresten
CA: 2 / 1
Laklaag: + / -
Grens stratigrafie
Einde boring / afgekapte boring
0
100 m
LLG 2012 2.0.25. Datum: 26/10/2021

Transect B

Appendix 2: GPR profiles 6 and 7

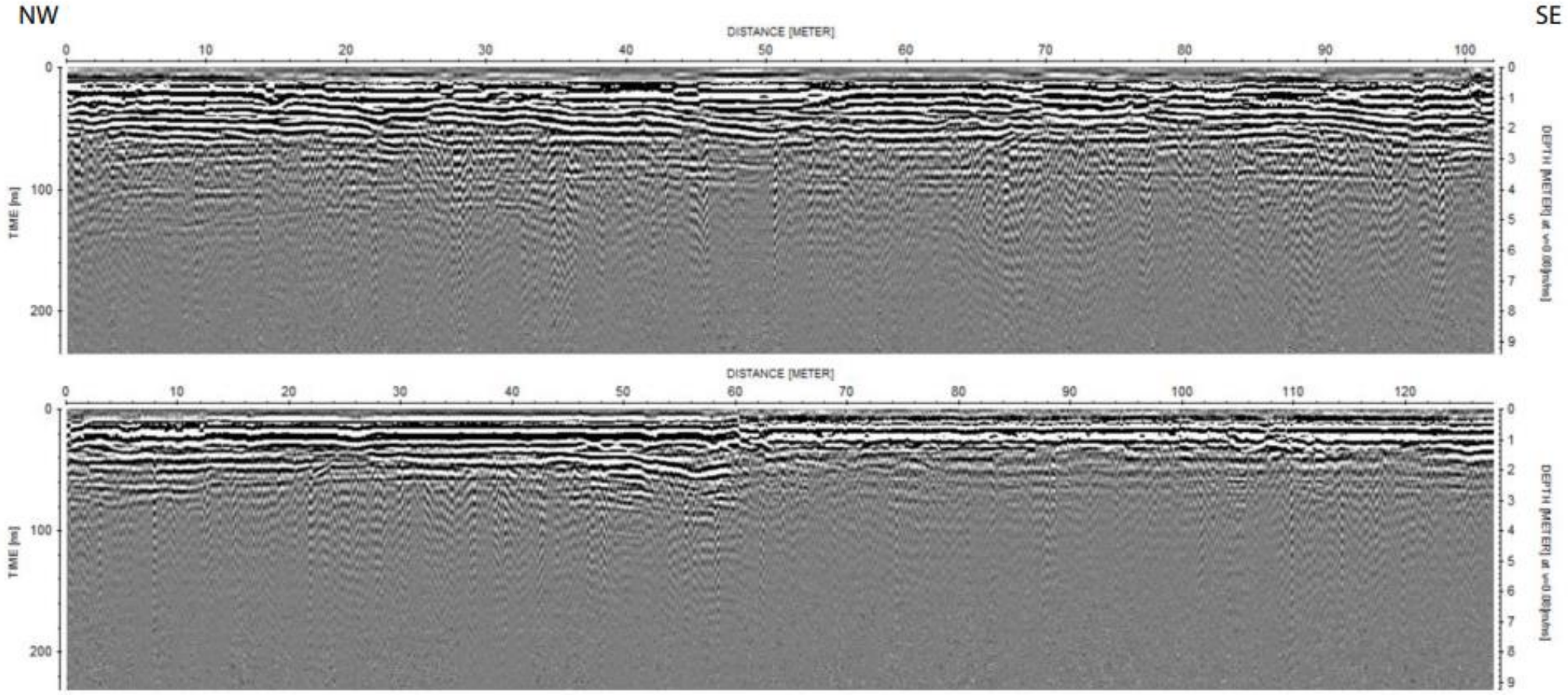

GPR profiles 6 (top) and 7 (bottom)